

Single-Stranded Hairpin Loop RNAs (loopmeRNAs) Potently Induce Gene Silencing through the RNA Interference Pathway

Krishna C. Aluri,[§] Dhrubajyoti Datta,[§] Scott Waldron, Nate Taneja, June Qin, Daniel P. Donnelly, Christopher S. Theile, Dale C. Guenther, Li Lei, Joel M. Harp, Pradeep S. Pallan, Martin Egli, Ivan Zlatev,^{*} and Muthiah Manoharan^{*}



Cite This: *J. Am. Chem. Soc.* 2024, 146, 28161–28173



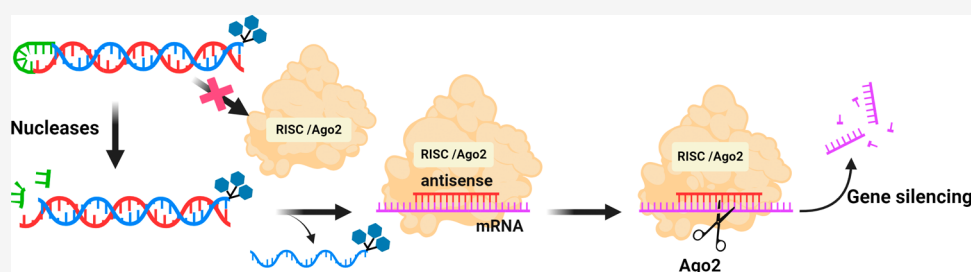
Read Online

ACCESS |

Metrics & More

Article Recommendations

Supporting Information



ABSTRACT: Synthetic small interfering RNAs conjugated to trivalent *N*-acetylgalactosamine (GalNAc) are clinically validated drugs for treatment of liver diseases. Incorporation of phosphorothioate linkages and ribose modifications are necessary for stability, potency, and duration of pharmacology. Although multiple alternative siRNA designs such as Dicer-substrate RNA, shRNA, and circular RNA have been evaluated in vitro and in preclinical studies with some success, clinical applications of these designs are limited as it is difficult to incorporate chemical modifications in these designs. An alternative siRNA design that can incorporate chemical modifications through straightforward synthesis without compromising potency will significantly advance the field. Here, we report a facile synthesis of GalNAc ligand-containing single-stranded loop hairpin RNAs (loopmeRNAs) with clinically relevant chemical modifications. We evaluated the efficiency of novel loopmeRNA designs in vivo and correlated their structure–activity relationship with the support of in vitro metabolism data. Sequences and chemical modifications in the loop region of the loopmeRNA design were optimized for maximal potency. Our studies demonstrate that loopmeRNAs can efficiently silence expression of target genes with comparable efficacy to conventional double-stranded siRNAs but reduced environmental and regulatory burdens.

INTRODUCTION

Since the award of the Nobel Prize for the discovery of the RNA interference (RNAi) pathway by Andrew Fire and Craig Mello in 2006,¹ tremendous progress has been made in harnessing the RNAi mechanism for human health. To date, six synthetic small interfering RNAs (siRNAs) that mediate gene silencing through the RNAi pathway have been approved by the US Food and Drug Administration (FDA), and several others are in clinical development.² The clinical pipeline of siRNAs is dominated by chemically modified, double-stranded siRNAs with 3′ overhangs at the antisense strand and sense strands conjugated to a trivalent *N*-acetylgalactosamine (GalNAc) ligand. The GalNAc ligand binds to the asialoglycoprotein receptor on hepatocytes to mediate liver-specific uptake of siRNA.^{3–8} Chemical modifications such as 2′-deoxy-2′-fluoro (2′-F) and 2′-*O*-methyl (2′-OMe) sugars and phosphorothioate (PS) linkages enhance the metabolic stability and reduce off-target effects. Chemical modifications to the nucleobases, sugars, and the phosphate backbone continue to be explored.^{9–19}

The conventional siRNA design is a 21/21 nucleotide duplex with a 3′ two-nucleotide overhang in the antisense strand (Figure 1a). In order to achieve higher efficiency of silencing or more cost-effective production, a number of other designs have been evaluated. One such strategy is altering the siRNA length. Khvorova et al. studied the use of asymmetric siRNA, typically 15/20 mers with five nucleotides in the 3′ overhang (Figure 1b) and demonstrated sustained target knockdown when chemical modifications like phosphorothioate linkages were optimized.²⁰ Chang et al. tested shorter siRNAs containing asymmetric 3′ antisense overhangs and demonstrated that siRNAs of 15–17 base pairs had activity.³²

Received: June 11, 2024
Revised: August 19, 2024
Accepted: August 21, 2024
Published: October 7, 2024



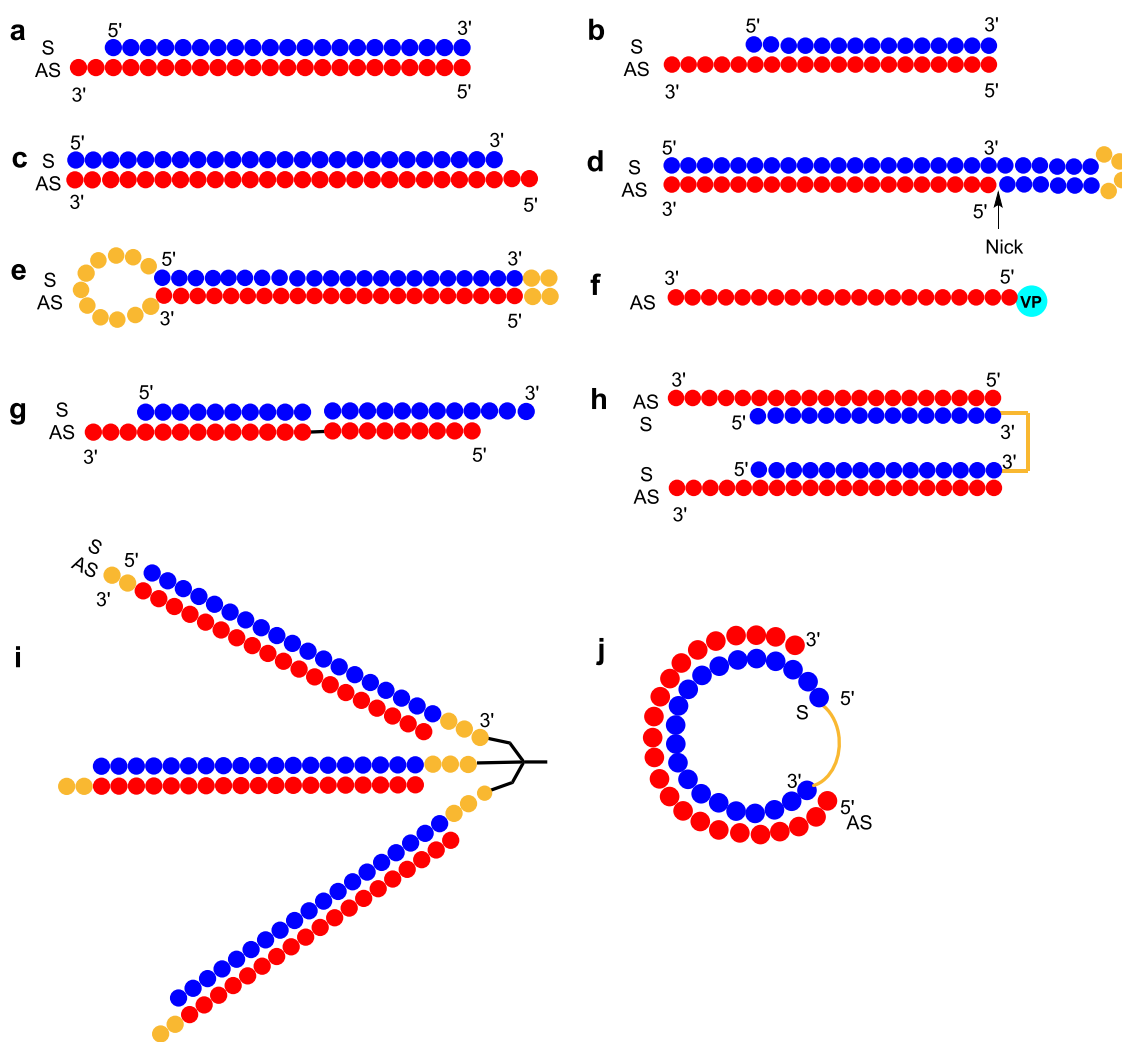


Figure 1. Conventional and selected alternative siRNA designs. (a) Cartoon of an siRNA part of the siRNA-GalNAc conjugate, the design used in clinically approved siRNAs (GalNAc ligand not shown); (b) asymmetric siRNA;²⁰ (c) Dicer-substrate (25/27 nucleotides) RNA;²¹ (d) Dicer-substrate nicked RNA;²¹ (e) shRNA;^{22–24} (f) ss-siRNA;^{25,26} (g) sisi siRNA;²⁷ (h) divalent siRNA;^{28,29} (i) branched trident siRNAs;³⁰ and (j) circular siRNA.³¹ Blue beads indicate nucleotides of the sense strand; red beads indicate nucleotides of the antisense strand; yellow beads indicate loop nucleotides or connecting linkages. VP indicates a 5'-(*E*)-vinylphosphonate. Structures of other chemical modifications are not shown here but are shown in Table 1.

Another siRNA design proposed by Rossi et al.^{33,34} is Dicer-substrate RNA, which is a double-stranded RNA duplex of 25–27 base pairs that are nicked by Dicer^{21,35} to yield 21 or 22-mer antisense strands (Figure 1c). The Dicer-substrate RNAs are delivered using nanoparticles or viral vectors, which might induce immunogenicity.³⁵ The Dicer-substrate nicked RNAs are duplexes with a prenicked antisense strand (Figure 1d). This design is used in GalXC siRNAs, which have sense strands functionalized with four GalNAc moieties.³⁶ Dicer-cleavable pre-microRNAs (pre-miRNAs) and short hairpin RNAs (shRNAs, Figure 1e) are additional classes of natural RNAs exploiting endogenous enzymatic processing of the miRNA pathway to generate the mature siRNA molecules.^{22–24,37} Therapeutic use of shRNA is limited because they are usually expressed from a viral vector,³⁸ which does not allow the incorporation of chemical modifications.^{39,40} Kim et al. prepared synthetic Dicer-substrate double-stranded RNAs of 25–30 base pairs, which can be chemically modified and show high potency, but these do not provide significant advantage over traditional siRNA designs.²¹ Single-stranded

siRNAs (ss-siRNA) designs were evaluated by Yu et al.²⁵ and Lima et al.²⁶ Of those tested, a 25-mer ss-siRNA containing 5'-(*E*)-vinylphosphonate (VP) was the most potent in vivo (Figure 1f). Wengel and co-workers tested a three-component design with a precleaved sense strand, which they termed sisi siRNAs (Figure 1g).²⁷ Divalent siRNAs, where two asymmetric siRNAs are connected via the sense strands by a tripolyethylene glycol linker, have also been evaluated (Figure 1h).^{28,29}

Another approach that has been explored is the use of supramolecular siRNA structures such as two-dimensional nanostructures in the form of nanosheets,⁴¹ Dicer-cleavable dumbbell-shaped nanocircular RNAs,⁴² branched siRNAs containing four strands,⁴³ and multiple designs of circular RNAs.^{44–47} Spherical nucleic acids of different structures have been studied by the Mirkin⁴⁸ and the Sleiman⁴⁹ laboratories. Higher-order V- and Y-shaped siRNAs have also been reported.^{50–52} Branched trident siRNA structures have also been made (Figure 1i).³⁰ We have synthesized and tested synthetic circular siRNA (Figure 1j), based on naturally

occurring circular RNAs in eukaryotes. When pharmacologically relevant chemical modifications such as 2'-F, 2'-OMe, VP, and PS were incorporated into the circular siRNAs, sustained knockdown of the target gene expression was observed.³¹

From a chemical synthesis standpoint, most of these designs require independent syntheses of the sense and antisense strands, both of which must be purified using a multistep approach. The strands are then annealed into a duplex that may be further purified prior to formulation. Even though this synthetic workflow is the current benchmark standard for GMP manufacturing of siRNAs, the process is complex, time-consuming, expensive, and raises environmental sustainability concerns.⁵³ According to the Environmental Protection Agency of the United States (<https://www.epa.gov/greenchemistry/basics-green-chemistry>), "Green chemistry is the design of chemical products and processes that reduce or eliminate the use or generation of hazardous substances. Green chemistry applies across the life cycle of a chemical product, including its design, manufacture, use, and ultimate disposal."

Here, we addressed the drawbacks of the previous designs with a novel design that we call the loopmeRNA. A loopmeRNA is synthesized as a chemically modified single strand that folds to form a hairpin that connects the 3' end of the antisense strand to the 5' end of the sense strand (Figure 2). The loop region in the loopmeRNA connects the 5' end of

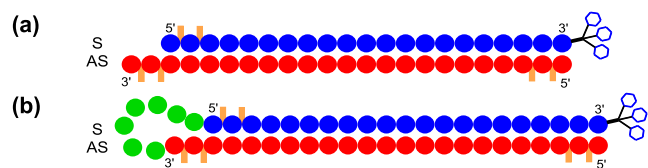


Figure 2. Schematics of (a) clinically approved siRNA and (b) loopmeRNA. Blue beads indicate nucleotides of the sense strand; red beads indicate nucleotides of the antisense strand; orange bars in each strand are phosphorothioate PS linkages; green beads depict loop nucleotides; and the blue hexagon triplet indicates GalNAc.

the sense strand to the 3' end of the antisense strand; in shRNAs,⁵⁴ Dicer-cleavable RNAs,^{21–24} and GalXC siRNAs,³⁶ the 5' end of the antisense strand is linked to the 3' end of the sense strand. LoopmeRNAs are synthesized as single strands, self-annealed due to sequence complementarity, and purified as single strands, resulting in lower cost and more environmentally friendly production. Delivery ligands such as triantennary GalNAc can be readily incorporated during the synthesis. We evaluated multiple loopmeRNA designs with different loop lengths and with different RNA, DNA, 2'-OMe, 2'-F, and PS contents in the loop region. We also evaluated the effect of the VP modification on the efficacy. Optimized loopmeRNAs have gene silencing activity comparable to that of conventional siRNA, and loopmeRNA metabolism is correlated with silencing efficiency. LoopmeRNAs warrant exploration as an alternative to conventional double-stranded siRNAs as the loopmeRNA design has comparable efficacy with half of the steps in the purification process.

RESULTS

Design of loopmeRNA Conjugates. Syntheses of chemically modified RNA-based therapeutics such as mRNAs⁵⁵ and guide RNAs⁵⁶ that are at least 100 nucleotides in length are now routinely performed on a large scale. This

prompted us to consider the design of long, single-stranded, chemically modified RNAs that contain sequences of both antisense and sense strands of an siRNA for use as therapeutic agents that act through the RNAi pathway. Ideally, this long RNA would be a substrate for endogenous nucleases and would include chemical modifications used in conventional siRNAs such as the enhanced stabilization chemistry¹⁴ and a triantennary GalNAc ligand for targeted hepatic delivery.¹³ This RNA must be metabolized in the endo/lysosome, releasing an siRNA antisense strand that can be loaded into the RISC to mediate the silencing of gene expression with potency comparable to that of a GalNAc-conjugated chemically modified siRNA molecule. We used an siRNA duplex containing triantennary GalNAc attached to a 3' sense strand targeting rodent *Ttr* as a template (ON-1) for our loopmeRNA designs. Multiple loopmeRNAs were designed that varied in the chemistry of the loop region that connected the 5' end of the sense strand to the 3' end of the antisense strand (Table 1). Our goal was to optimize the loop region to ensure stability in circulation and to modulate cleavage into mature siRNA after internalization in the liver.

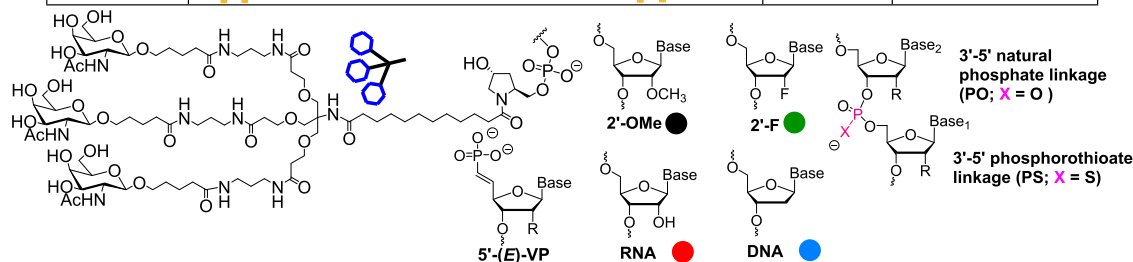
We tested loopmeRNAs with loops containing all 2'-OMe-modified nucleotides (ON-2), a design that should be stable against endogenous nucleases; with loops containing three 2'-F-modified nucleotides (ON-3), which are labile in the liver; and with loops containing either RNA or DNA residues (ON-4, ON-5, ON-6, and ON-7), which should be even more labile than the loopmeRNA with 2'-F-modified nucleotides. We hypothesized that differences in nucleolytic susceptibility would impact the rate at which loopmeRNA was cleaved into sense and antisense strands. Finally, to provide maximal stability, we synthesized a loopmeRNA with a 2'-OMe-modified loop region with all PS linkages (ON-8). As VP placed at the 5' end of antisense strand enhances efficacy and stability of conventional double-stranded siRNA,⁵⁷ we included a loopmeRNA with VP and a 2'-OMe loop (ON-9), a loopmeRNA with VP and a 2'-F-containing loop (ON-10) and the VP modified ON-8 (ON-11, 2'-OMe loop with PS linkages). As controls, we used conventional siRNAs without VP (ON-1) and with the VP modification (ON-12).

Synthesis and Purification of loopmeRNAs. The well-established current manufacturing process for double-stranded synthetic siRNA duplexes is based on the individual syntheses of the two oligonucleotides, the sense strand and the antisense strand (Scheme 1a). After the solid-phase synthesis is completed, the crude strands are cleaved from the solid support, and after ultrafiltration, each individual strand is purified by ion-exchange HPLC and desalted by ultrafiltration. The purified sense and antisense strands are mixed in an equimolar ratio to generate the duplex siRNA (Scheme 1a). The loopmeRNA is produced in a single solid-phase synthesis (Scheme 1b), reducing the downstream process steps into a single stream workflow, instead of the two for a conventional siRNA (Scheme 1), eliminating half of the steps. Given the high overall crude yields observed for the synthesis of long (~50 nucleotide) oligonucleotides and the single HPLC purification step, the loopmeRNA compounds were synthesized with yields similar to those of standard siRNAs, with half of the processing and purification downstream steps.

In Vivo Activity of loopmeRNA Conjugates. We evaluated the efficacy of silencing of the mouse *Ttr* mRNA in C57BL/6 mice. LoopmeRNAs and control siRNAs were administered in a single subcutaneous dose with groups of

Table 1. Control siRNAs and loopmeRNAs Used in This Study

Entry	Structure [#]	Mass (M-H) ⁻	
		Calcd.	Obsd.
ON-1		16310.12 (Duplex)	16310.05 (Duplex)
ON-2		18744.96	18743.43
ON-3		18770.94	18769.43
ON-4		18746.99	18743.24
ON-5		18514.73	18510.51
ON-6		18730.99	18726.87
ON-7		18509.81	18506.74
ON-8		17404.29	17402.86
ON-9		18820.97	18819.31
ON-10		18846.94	18845.22
ON-11		17480.29	17478.87
ON-12		16386.10 (Duplex)	16389.20 (Duplex)

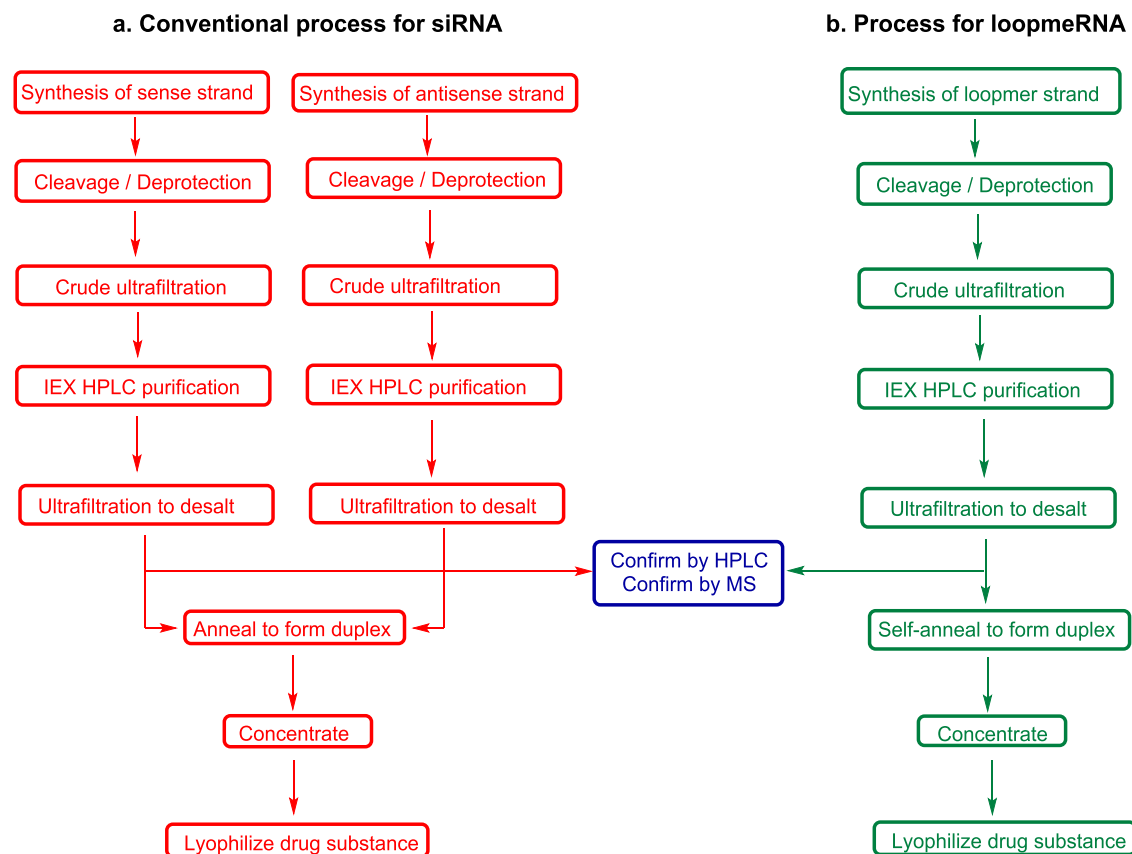


[#]In the duplex regions, the upper strand is the sense strand written in the 5' to 3' direction and the lower strand is the antisense strand written 3' to 5'. The chemical structures of the oligonucleotide building blocks are indicated by beads: black, 2'-Ome; green, 2'-F; blue, DNA; and red, RNA. Orange lines indicate PS linkages; all other linkages are phosphate. VP indicates (E)-VP. The 3' ends of sense strands or loopmeRNAs are conjugated to trivalent GalNAc.

mice given 1, 0.4, or 0.2 mg/kg of the siRNA or loopmeRNA. At the highest dose of 1 mg/kg, significant reductions in TTR protein were observed in mice treated with all loopmeRNAs, but differences in reductions were minimal, making it impossible to rank order the various designs (Figure 3a). At a dose of 0.4 mg/kg, the reduction in TTR caused by ON-11 was delayed relative to other designs; nadir was reached at 21 days postdose with ON-11, whereas other loopmeRNA designs reached a nadir at day 14 with comparable reductions (Figure 3b). At the lowest dose of 0.2 mg/mL, clear differences in loopmeRNA potencies were observed (Figure 3c). ON-5, which has a loop containing RNA and DNA, and ON-10, which has a 2'-F loop with a 5'-(E)-VP, had the highest

silencing activities comparable to that of the control siRNA (~80% reduction in TTR). The loopmeRNA with a DNA loop (ON-7) had the next highest activity potency (~60% reduction), followed by ON-3 (~55%), ON-6 (50%), and ON-9 (~50%). LoopmeRNAs with 2'-Ome (ON-2) and 2'-Ome and PS modifications (ON-11) in the loops were the least potent (~30% and 20%, respectively). At the 0.2 mg/kg dose, we did not observe the delayed activity by ON-11 seen at a higher dose of 0.4 mg/kg dose. The difference in potency between siRNA ON-1 without VP and the siRNA ON-12 with VP was not significant (Figure 4a), whereas VP did improve potencies of loopmeRNAs with stable (ON-2 vs. ON-9) and labile loops (ON-3 vs. ON-10) (Figure 4b).

Scheme 1. Synthesis and Purification Steps for the Manufacturing of (a) Conventional Double-Stranded siRNA Duplexes and (b) loopmeRNAs



In Vitro Metabolism of loopmeRNAs Is Governed by Chemical Modifications. We next evaluated the metabolic stabilities of loopmeRNAs and control siRNAs in plasma and liver homogenates. Rat plasma and rat liver homogenates were used in this analysis, as rat matrices more closely mimic long-term in vivo metabolism and clearance in humans than do mouse matrices. The siRNAs were incubated in rat plasma for 24 h at 37 °C, and samples were analyzed using HPLC followed by mass spectrometry. No significant metabolism of loopmeRNAs or the controls was observed in plasma (Figure S1 and Table S2).

LoopmeRNAs were incubated in rat liver homogenates for 24 h at 37 °C, and metabolite profiling was performed using HPLC followed by mass spectrometry. Data are summarized in Tables 1 and 2 and Figure 5. There was no significant metabolism of the control siRNA ON-1 antisense strand. Loss of one GalNAc saccharide from the trivalent ligand was the only major sense strand metabolite observed for the parent ON-1. The percent of full-length loopmeRNAs remaining varied from 0% for the loopmeRNA with RNA and DNA residues in the loop (ON-5) to 85.4% for the “super stable” (Table 2) loopmeRNA with 2'-OMe residues with PS linkages (ON-8). The major metabolites observed for ON-2, which has a 2'-OMe loop, did not result from cleavage in the loop region but rather from cleavages at residues 39–41, (for the numbering of residues in the loopmeRNA, see Supporting Information, Table S3) which is a 2'-F triplet in the sense region. The major metabolite observed for ON-3, which has 2'-F in the loop, was due to cleavage at nucleotide 23 in the antisense region, and multiple additional cleavages in the loop

region also released the antisense strand. The major metabolites for ON-4, which has a single RNA residue and two DNA residues in the loop, were the 23-mer antisense strand and a 22-mer sense strand; the 22-mer resulted from cleavage at position 31. For ON-5, which has three RNA residues and four DNA residues in the loop, the major metabolites were the 23-mer antisense strand and a 23-mer sense strand, which resulted from cleavage at position 30. ON-6 with three DNA residues in an otherwise 2'-OMe loop was also cleaved to release a 23-mer antisense strand, but no other metabolites indicative of cleavage within the loop were observed. ON-7, which has a DNA loop, was cleaved at positions 23 and 31. No cleavage in the loop region was observed for ON-8, which has PS linkages in the 2'-OMe loop region; multiple minor metabolites were observed that resulted from cleavage at 2'-F-modified nucleotides. In summary, the introduction of DNA, RNA, or 2'-F RNA in the loop with a length of 3 to 7 nucleotides (if we add the length of the antisense overhang, it could be considered as 5 to 9 nucleotides) increased the metabolism of the loop region, resulting in the release of the antisense strand as a metabolite, which was essential for efficient gene knockdown. On the other hand, 2'-OMe RNA and/or PS linkages decreased the metabolism of the loop and negatively impacted the RNAi activity.

ON-9, the 5' VP-modified counterpart of ON-2, which has a 2'-OMe loop, had a metabolism pattern similar to that of ON-2 with no cleavages in the 2'-OMe-containing loop region. ON-10, the 5' VP-modified counterpart of ON-3 that has 2'-F in the loop was cleaved to release a 23-mer antisense strand

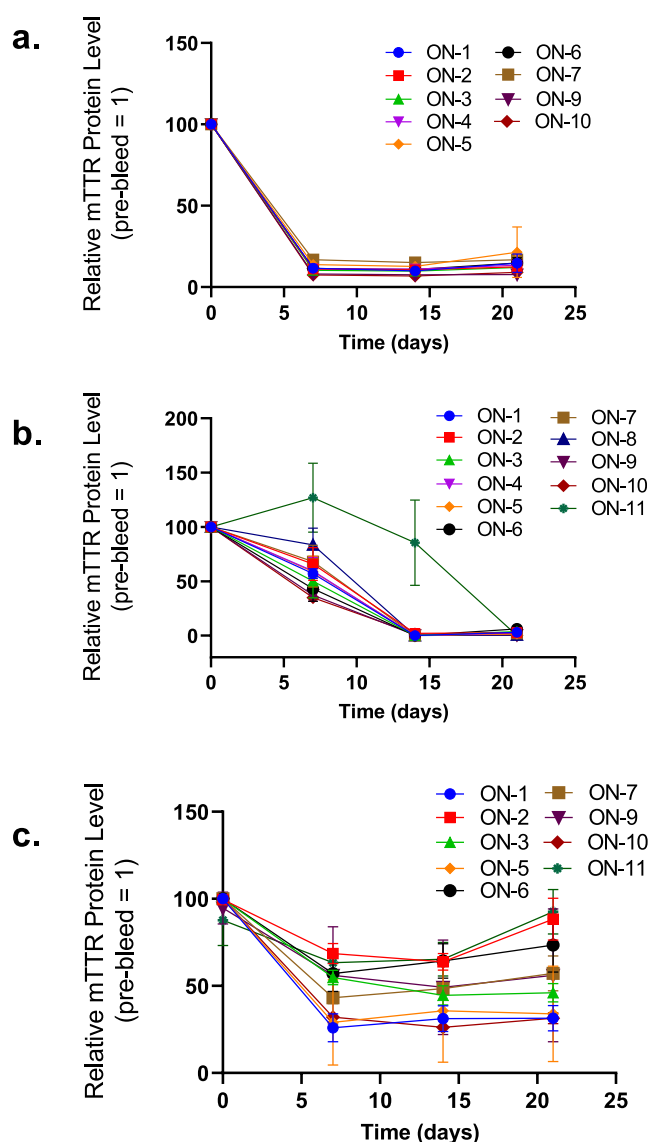


Figure 3. LoopmeRNAs reduce TTR expression in mice. TTR protein levels over time in mice treated with (a) 1 mg/kg, (b) 0.4 mg/kg, and (c) 0.2 mg/kg in indicated siRNA. Mice were treated on day 0, and serum was collected on days 0 (predose), 7, 14, and 21 and analyzed for TTR protein. TTR levels are plotted relative to those of PBS-treated mice. Error bars are \pm SD ($n = 3$).

and a 21-mer sense strand and also had multiple cleavages at residues 29, 30, and 32, similar to those of ON-3. ON-11, the 5' VP-modified loopmeRNA with PS linkages in the 2'-OME loop region, was not metabolized in the loop but, like its counterpart ON-8, was cleaved at some 2'-F residues. For ON-2 and ON-9, no 23-mer antisense strand was detected. For the loopmeRNA with the 2'-F-containing loop, we observed an increase in the number of cleavage sites in the VP-modified ON-10 compared to ON-3, which lacks VP. For both, the 23-mer antisense metabolite was detected. Therefore, VP did not alter the metabolism of the loopmeRNA with a 2'-OME loop but did slightly enhance the metabolism of the loopmeRNA with a 2'-F loop.

Correlation of Metabolism with TTR Reduction. We correlated the amounts of various metabolites, determined by quantification of intensities of ion chromatographic peaks from experiments performed in rat liver homogenates, with

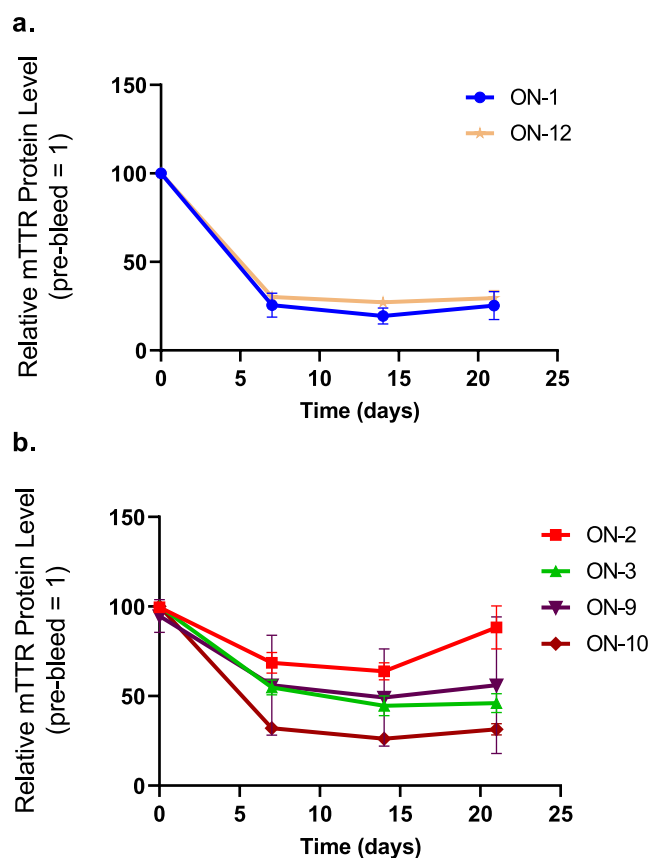


Figure 4. VP improves the loopmeRNA potency. TTR protein levels over time in mice treated with 0.2 mg/kg (a) control siRNAs ON-1 without and ON-12 with VP and (b) loopmeRNAs ON-2 and ON-9 without and ON-3 and ON-10 with VP. Mice were treated on day 0, and serum was collected on days 0 (predose), 7, 14, and 21 and analyzed for TTR protein. TTR levels are plotted relative to PBS-treated mice. Error bars are \pm SD ($n = 3$).

reductions in TTR at day 7 in mice given a 0.2 mg/kg dose of loopmeRNA. Loss of the full-length loopmeRNA was inversely correlated with percent TTR remaining with a Pearson r of -0.8300 ($P = 0.01$) (Figure 6). The formation of a 22- or 23-mer metabolite corresponding to the antisense strand was statistically significantly correlated with the percent TTR remaining with a Pearson r of 0.8118 ($P = 0.04$) (Figure S2). Thus, potency is optimal when the loopmeRNA is metabolized to release the antisense strand.

The Ago2 PAZ Domain Cannot Accommodate an Intact RNA Hairpin Loop Structure. Interactions between the residues of the 3'-terminal overhang of the antisense strand and the PAZ domain in crystal structures for complexes of full-length human Ago2 are not well defined.^{58–60} Moreover, such structures contain only residues that map to the 3' half of the strand, with no density corresponding to the 5' half of the strand. Thus, the relative orientations of the 5' terminus of the sense strand and the 3' terminus of the antisense strand captured by PAZ are not defined in these complexes. The only crystal structure of a complex between a separate PAZ domain and an RNA duplex with a 3'-terminal dinucleotide overhang is for human Ago1.⁵⁸ To fill this void, we determined the 2.2 Å-resolution crystal structure of a complex between human Ago2 PAZ (amino acids Ala-227 to Cys-352) and the RNA 9-mer 5'-CGU GAC UCU-3' that forms a duplex with a 3'-terminal CU overhang that is lodged in the PAZ binding pocket (Figures

Table 2. Sequences, Descriptions, Degradation Profiles, and Activities of Control siRNAs and loopmeRNAs

Entry	Structure [#]	Loop length (nucleotides)	Description	Percent full-length strand at 24 h in liver homogenate	% TTR protein remaining in serum on day 7 (dose in mg/kg) [†]
ON-1		No loop	Control siRNA		30.2 (0.2)
ON-2			Stable loop	52.7	68.6 (0.2)
ON-3			Semi labile loop	0.0	54.9 (0.2)
ON-4			Semi labile loop	0.0	59.5 (0.4)
ON-5			Super labile loop	0.0	29.0 (0.2)
ON-6			Labile loop	19.2	57.1 (0.2)
ON-7			Labile loop	3.0	43.2 (0.2)
ON-8			Super stable loop	85.4	83.5 (0.4)
ON-9			Stable loop with VP	52.1	56.9 (0.2)
ON-10			Semi labile loop with VP	4.0	32.1 (0.2)
ON-11			Super stable loop with VP	67.5	63.3 (0.2)
ON-12		No loop	Control siRNA with VP		25.6 (0.2)

[#]Same as Table 1. [†]Data from mice dosed SC siRNA controls or loopmeRNA designs, data from Figures 3b,c and 4a,b.

S3–S6 and Table S1). The complex adopts a dumbbell-like shape with duplex ends bound to separate PAZ domains (Figure 7a). A comparison between the binding modes of 3'-overhanging nucleotides by the human Ago2 and Ago1 PAZ domains is depicted in Figure S7.

Our crystal structure of the PAZ domain bound to a short duplex with a 3'-terminal dinucleotide overhang allows an accurate assessment of the spacing between the 3'-OH of the antisense strand trapped in the PAZ binding pocket and the 5' end of the sense strand located on the PAZ surface. As shown in Figure 7b, the direct distance between P(S2), the 5' end of the sense strand, and O3'(AS23), the 3' end of the antisense strand, is 24 Å. Thus, seven nucleotides are not sufficient to connect these termini when the two strands are paired and bound to the PAZ domain. Further, the O3' of the terminal residue of the antisense strand is buried inside the PAZ domain, making a connection impossible unless the con-

formation of AS23 were altered so that the O3' points outward. This analysis supports the hypothesis that Ago2 binding and silencing are preceded by the metabolism of the loopmeRNA that releases an antisense strand, as indicated by the inverse correlation between full-length loopmeRNA and silencing in mice.

DISCUSSION

LoopmeRNA Design Considerations and Avenues of Future Optimization. We describe here the optimization of a new class of fully chemically modified GalNAc-conjugated siRNAs, the loopmeRNAs. We tested constructs with loop regions of various lengths (three to seven nucleotides) containing RNA, DNA, 2'-OMe, and 2'-F analogues with and without PS linkages with the aim of tailoring nucleolytic degradation of the loop region to confer a pro-drug property. We correlated gene silencing activity in mice with metabolic

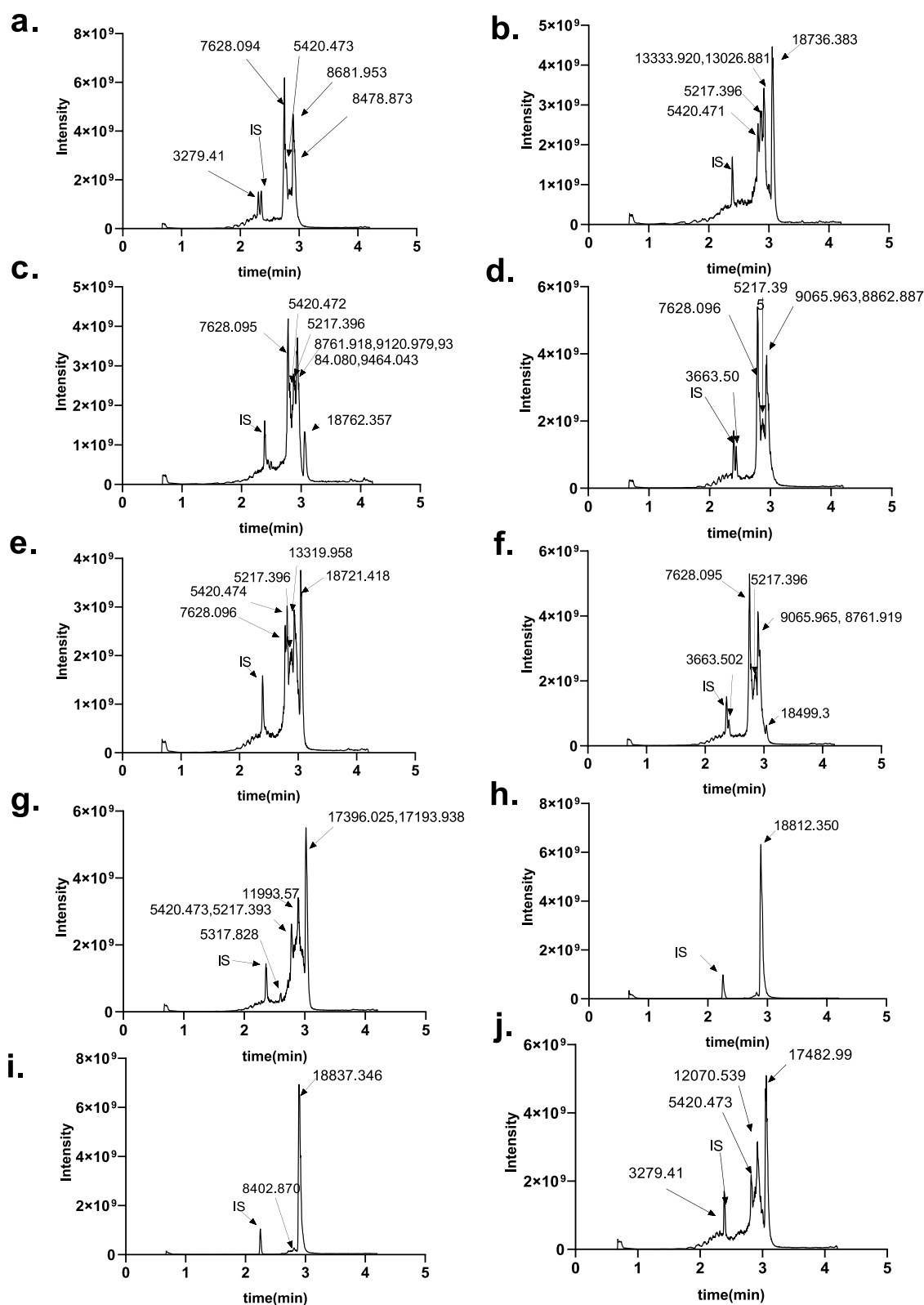
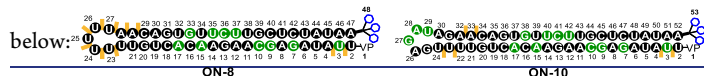


Figure 5. Loop sequence and chemistry influences metabolism of loopRNAs. Ion chromatograms of samples of (a) ON-1, (b) ON-2, (c) ON-3, (d) ON-5, (e) ON-6, (f) ON-7, (g) ON-8, (h) ON-9, (i) ON-10, and (j) ON-11 after incubation in rat liver homogenate for 24 h at 37 °C. The residue identifier in the text is illustrated by taking examples ON-8 and ON-10



cleavage of the hairpin loop to identify important characteristics of an active loopRNA. The designs described in this work were not exhaustive but did define several critical

parameters. Our data indicate that native DNA and RNA nucleotides or 2'-F nucleotides in the loop region destabilize the loop, leading to efficient nuclease cleavage and release of

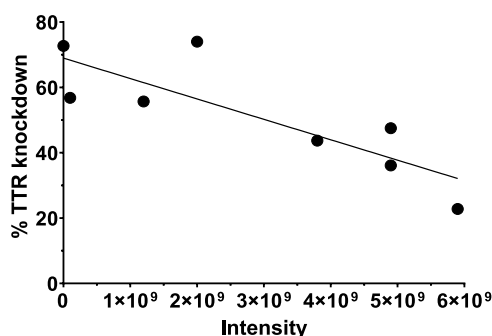


Figure 6. Percent TTR reduction in vivo inversely correlates with the amount of full-length loopmeRNA remaining in rat liver homogenate. Plot of TTR remaining at day 7 in mice treated with 0.2 mg/kg dose of loopmeRNA vs. signal intensity due to full-length loopmeRNA after incubation in rat liver homogenate for 24 h.

double-stranded siRNA capable of loading into RISC for gene silencing. Using modifications such as 2'-OMe and PS makes the loop region more stable and less susceptible to nuclease cleavage, in turn reducing the activity of loopmeRNA. We observe a correlation between the efficiency of cleavage within the loop region of the loopmeRNA and gene silencing efficiency. Further, our analysis of a crystal structure of the PAZ domain bound to a short RNA duplex supports the hypothesis that the loopmeRNA must be processed, likely by nonspecific nucleases rather than Dicer, prior to incorporation into the RISC (Figure 8).

A mixed chemistry and a combination of purines and pyrimidines patterns^{61–63} were deployed based on our metabolite analysis (Supporting Information), where effective cleavage of the hairpin was observed for the most tissue labile loopmeRNAs, eventually correlating with the highest level of in vivo mRNA silencing potency. In addition, the use of larger hairpin loops in combination with directed purine-pyrimidine cleavage sites^{61–63} demonstrated the most promising potency in this approach.

Synthesis and Purification of loopmeRNAs: Potential Advantages and Concerns. LoopmeRNAs are synthesized and purified as a single strand, thus increasing throughput and reducing the overall manufacturing time and cost. The current manufacturing process for synthetic siRNA duplexes is based on the individual preparation of each strand, including synthesis, cleavage from support and deprotection, ultrafiltration, ion-exchange HPLC purification, and final desalting by ultrafiltration, prior to the annealing of the two strands to generate the duplex. This process is the standard for the supply chain of the six clinically approved siRNA therapeutics and those in clinical testing. Cost of goods, raw materials availability, and scale-up of the HPLC purification may limit the use of RNAi in indications with large populations as metric ton annual production goals are still elusive. New methods and new chemical designs that reduce costs will allow a wider use of these agents. As described in this work, the preparation of loopmeRNAs involves a single synthesis and a single HPLC purification and does not require annealing, thereby eliminating half of the steps in the production process relative to an siRNA duplex.

Process development and optimization were beyond the scope of this work, but it is worth noting that the synthesis of a 50-mer oligonucleotide with the current methods of stepwise solid-phase phosphoramidite synthesis is expected to result in

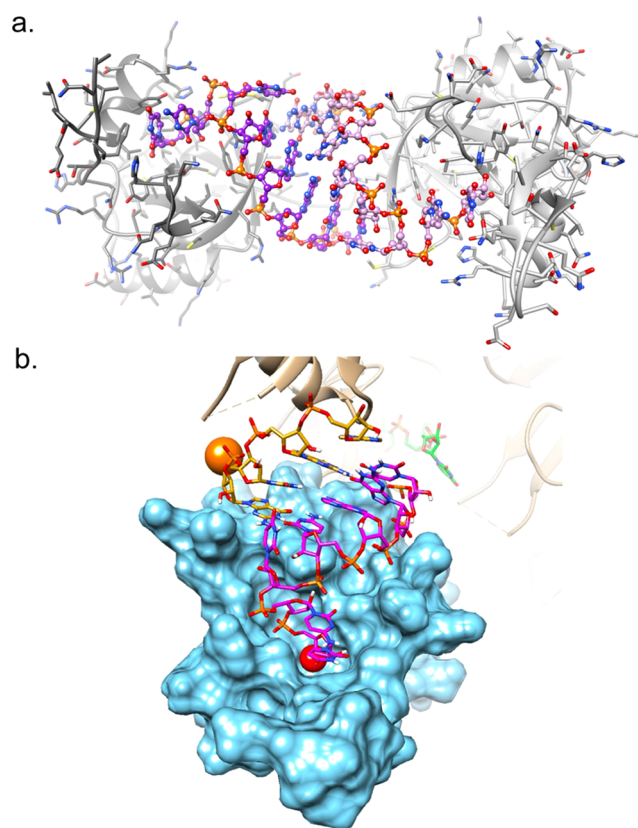


Figure 7. Ago2 binding and silencing are preceded by the metabolism of the loopmeRNA. (a) Crystal structure of the complex between the Ago2 PAZ domain and the RNA 9-mer 5'-CGU GAC UCU-3'. In the crystal, two oligoribonucleotides form a duplex with mismatch pairs and 3'-terminal CU overhangs that are captured by PAZ domains bound to opposite ends of the RNA duplex. (b) Relative orientations of the siRNA antisense and sense strands bound to the Ago2 PAZ domain. Carbon atoms of the sense strand are colored in goldenrod and those of the antisense strand are colored in magenta; the PAZ domain surface is shown in light blue. The first bridging phosphate (P2) of the sense strand is highlighted as an orange sphere (phosphorus), and the O3' atom of the 3'-terminal residue of the antisense strand (U23) is highlighted as a red sphere. The model depicted was generated by overlaying the Ago2 PAZ domain (residues 226–348) bound to a sense-antisense duplex and the complex between Ago2 and miR-20a⁵⁹ (PDB 4F3T; beige protein ribbons and RNA carbon atoms colored in green). In the latter structure, there is no sense strand; similarly, there are no sense strand residues beyond 12 in published structures that contain RNA duplexes (meaning S1–S11 are missing, e.g., in the complex with PDB ID 4W5T).⁶⁰ The green residue is AS10; at AS17, the strand reappears in the structure and then ends at AS19 (G) and AS20 (G). These last four residues have been deleted from the overlay, as they would partially obscure the magenta residues from the structure of our complex with the Ago2 PAZ domain alone.

significantly lower yield of crude full-length product than obtained for a 23-mer oligonucleotide (i.e., for a stepwise coupling yield of 98%, a 50-mer would yield a crude product of 36.4% vs. 62.8% for a 23-mer). Lower crude yields likewise lead to more difficult purifications. However, the elimination of an HPLC purification step is a significant benefit, since the HPLC stationary phase and solvents are some of the most expensive and nongreen reagents in the oligonucleotide manufacturing process.

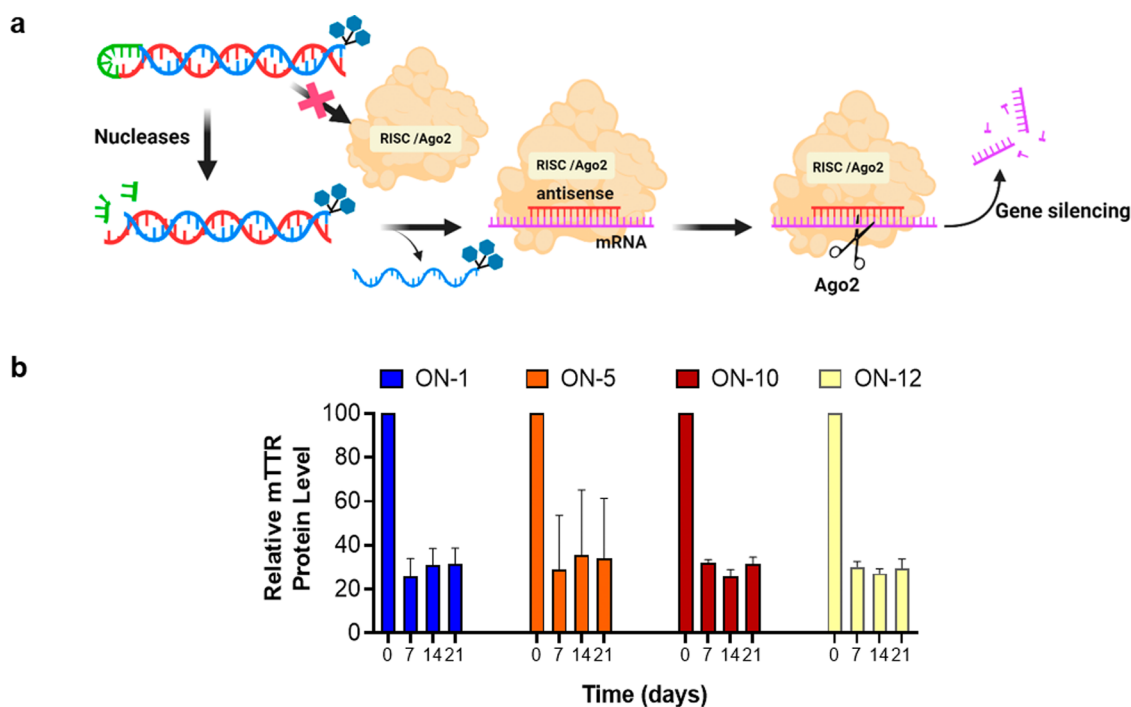


Figure 8. (a) Cartoon illustration of loopmeRNA processing and the mediation of gene silencing through the RNAi mechanism. An intact loopmeRNA is not incorporated into the RISC. Once the loop is cleaved to release the siRNA, binding to RISC occurs and the antisense strand recognizes a target mRNA to mediate gene silencing. (b) Comparative *Ttr* silencing in mice for loopmeRNA ON-5 and ON-10 compared to that of corresponding control siRNAs ON-1 and ON-12, respectively, when administered at a 0.2 mg/kg dose.

Future Optimization Opportunities. Enzymatic synthesis methods currently in development may greatly streamline the efficacy of synthesis and coupling yields,^{64,65} and novel designs such as loopmeRNA could be synthesized using these methods. Likewise, future optimizations of solid-phase synthesis methods and reagents, such as solid support material (controlled-pore glass, polymer supports, and PEGs), their loading capacity, and pore size, as well as novel coupling reagents are expected to enhance loopmeRNA synthesis performance, yields, and product quality.⁶⁴

Going beyond GalNAc Conjugates? In the present work, to demonstrate the validity of the loopmeRNA platform, GalNAc conjugates were used. GalNAc sugars are hydrophobic. More recently, lipid conjugates have entered the clinic. These hydrophobic siRNAs⁶⁶ are expected to get an additional synthetic advantage from the loopmeRNA approach: purification of the approximately 50-nucleotide loopmeRNA linked to a lipid will be simpler than purification of a lipid-conjugated 21-nucleotide siRNA sense strand.

CONCLUSIONS

Given the clinical successes of siRNA therapeutics in the treatment of previously untreatable as well as prevalent diseases, there has been an increased focus on developing new modalities that can reduce the expression of target genes more efficiently and more cost-effectively than the currently employed siRNA designs. In this study, we introduced a novel loopmeRNA design and performed structure–activity relationship experiments to understand the effect of chemical modifications within the loop region on the gene silencing activity. Labile residues such as DNA, RNA, and 2'-F RNA increased the metabolism of the loop region, resulting in the release of the antisense strand as a metabolite, which was essential for efficient gene knockdown. The loopmeRNA

design streamlines the manufacturing process, potentially reducing the cost of production and environmental and regulatory burdens. We expect that the safety of the loopmeRNA should be acceptable, as no novel chemical entities were introduced. Further optimization and more thorough evaluation of loopmeRNAs could also open possibilities of expanding these constructs to other extrahepatic applications beyond the GalNAc conjugates targeted to the liver (Figure 1). Now that we have established that loopmeRNAs are potent and effective in vivo, the synthetic methodology described herein as well as alternate methods of synthesis such as enzymatic methods⁶⁷ or new solid supports and reagents can also provide additional validation for these novel designs to move forward clinically.⁶⁸

ASSOCIATED CONTENT

Supporting Information

The Supporting Information is available free of charge at <https://pubs.acs.org/doi/10.1021/jacs.4c07902>.

Additional experimental details, materials, and methods, including photographs of the experimental setup, major metabolites details of siRNA or loopmeRNA, correlation of metabolite profile to activity graph, details of crystal structure, and modeling studies (PDF)

AUTHOR INFORMATION

Corresponding Authors

Ivan Zlatev – Alnylam Pharmaceuticals, Inc., Cambridge, Massachusetts 02142, United States; orcid.org/0000-0003-2797-3032; Phone: +1-617-682-4164; Email: izlatev@alnylam.com

Muthiah Manoharan – Alnylam Pharmaceuticals, Inc., Cambridge, Massachusetts 02142, United States;

orcid.org/0000-0002-7931-1172; Phone: +1-617-551-8319; Email: mmanoharan@alnylam.com

Authors

Krishna C. Aluri – Alnylam Pharmaceuticals, Inc., Cambridge, Massachusetts 02142, United States

Dhrubajyoti Datta – Alnylam Pharmaceuticals, Inc., Cambridge, Massachusetts 02142, United States

Scott Waldron – Alnylam Pharmaceuticals, Inc., Cambridge, Massachusetts 02142, United States

Nate Taneja – Alnylam Pharmaceuticals, Inc., Cambridge, Massachusetts 02142, United States

June Qin – Alnylam Pharmaceuticals, Inc., Cambridge, Massachusetts 02142, United States

Daniel P. Donnelly – Alnylam Pharmaceuticals, Inc., Cambridge, Massachusetts 02142, United States

Christopher S. Theile – Alnylam Pharmaceuticals, Inc., Cambridge, Massachusetts 02142, United States

Dale C. Guenther – Alnylam Pharmaceuticals, Inc., Cambridge, Massachusetts 02142, United States

Li Lei – Department of Biochemistry, School of Medicine, Vanderbilt University, Nashville, Tennessee 37232, United States

Joel M. Harp – Department of Biochemistry, School of Medicine, Vanderbilt University, Nashville, Tennessee 37232, United States

Pradeep S. Pallan – Department of Biochemistry, School of Medicine, Vanderbilt University, Nashville, Tennessee 37232, United States

Martin Egli – Department of Biochemistry, School of Medicine, Vanderbilt University, Nashville, Tennessee 37232, United States; orcid.org/0000-0003-4145-356X

Complete contact information is available at: <https://pubs.acs.org/10.1021/jacs.4c07902>

Author Contributions

[§]K.C.A. and D.D. are first authors with equal contribution.

Funding

This work was funded by Alnylam Pharmaceuticals.

Notes

The authors declare no competing financial interest. K.C.A., D.D., S.W., N.T., J.Q., D.P.D., C.S.T., D.C.G., I.Z., and M.M. are currently or were during the time this work was conducted, employees of Alnylam Pharmaceuticals.

ACKNOWLEDGMENTS

We dedicate this paper to our dear friend and colleague Klaus Charisse for his contributions to Alnylam Drug Discovery and leadership of Synthelytics team over the past 21 years (2003–2024). We also thank our colleagues Lubo Nechev, Martin Maier, Ingo Roehl, and Philipp Hadwiger for useful discussions.

REFERENCES

- (1) Fire, A.; Xu, S.; Montgomery, M. K.; Kostas, S. A.; Driver, S. E.; Mello, C. C. Potent and specific genetic interference by double-stranded RNA in *Caenorhabditis elegans*. *Nature* **1998**, *391* (6669), 806–811.
- (2) Setten, R. L.; Rossi, J. J.; Han, S.-P. The current state and future directions of RNAi-based therapeutics. *Nat. Rev. Drug Discovery* **2019**, *18*, 421–446.
- (3) Nair, J. K.; Willoughby, J. L.; Chan, A.; Charisse, K.; Alam, M. R.; Wang, Q.; Hoekstra, M.; Kandasamy, P.; Kel'in, A. V.; Milstein, S.;

Taneja, N.; O'Shea, J.; Shaikh, S.; Zhang, L.; van der Sluis, R. J.; Jung, M. E.; Akinc, A.; Hutabarat, R.; Kuchimanchi, S.; Fitzgerald, K.; Zimmermann, T.; van Berkel, T. J.; Maier, M. A.; Rajeev, K. G.; Manoharan, M. Multivalent N-acetylgalactosamine-conjugated siRNA localizes in hepatocytes and elicits robust RNAi-mediated gene silencing. *J. Am. Chem. Soc.* **2014**, *136* (49), 16958–16961.

(4) Springer, A. D.; Dowdy, S. F. GalNAc-siRNA Conjugates: Leading the Way for Delivery of RNAi Therapeutics. *Nucleic Acid Ther.* **2018**, *28* (3), 109–118.

(5) Fitzgerald, K.; Kallend, D.; Simon, A.; et al. A Highly Durable RNAi Therapeutic Inhibitor of PCSK9. *N. Engl. J. Med.* **2017**, *376* (18), No. e38.

(6) Pasi, K. J.; Rangarajan, S.; Georgiev, P.; Mant, T.; Creagh, M. D.; Lissitchkov, T.; Bevan, D.; Austin, S.; Hay, C. R.; Hegemann, I.; Kazmi, R.; Chowdary, P.; Gercheva-Kyuchukova, L.; Mamonov, V.; Timofeeva, M.; Soh, C. H.; Garg, P.; Vaishnav, A.; Akinc, A.; Sorensen, B.; Ragni, M. V. Targeting of Antithrombin in Hemophilia A or B with RNAi Therapy. *N. Engl. J. Med.* **2017**, *377* (9), 819–828.

(7) Zimmermann, T. S.; Karsten, V.; Chan, A.; Chiesa, J.; Boyce, M.; Bettencourt, B. R.; Hutabarat, R.; Nochur, S.; Vaishnav, A.; Gollob, J. Clinical Proof of Concept for a Novel Hepatocyte-Targeting GalNAc-siRNA Conjugate. *Mol. Ther.* **2017**, *25* (1), 71–78.

(8) Sardh, E.; Harper, P.; Balwani, M.; Stein, P.; Rees, D.; Bissell, D. M.; Desnick, R.; Parker, C.; Phillips, J.; Bonkovsky, H. L.; Vassiliou, D.; Penz, C.; Chan-Daniels, A.; He, Q.; Querbes, W.; Fitzgerald, K.; Kim, J. B.; Garg, P.; Vaishnav, A.; Simon, A. R.; Anderson, K. E. Phase 1 Trial of an RNA Interference Therapy for Acute Intermittent Porphyria. *N. Engl. J. Med.* **2019**, *380* (6), 549–558.

(9) Elkayam, E.; Joshua-Tor, L.; Brown, C. R.; Theile, C. S.; Willoughby, J. L.; Parmar, R.; Manoharan, M. siRNA carrying an (E)-vinylphosphonate moiety at the 5' end of the guide strand augments gene silencing by enhanced binding to human Argonaute-2. *Nucleic Acids Res.* **2017**, *45* (6), 3528–3536.

(10) Janas, M. M.; Jiang, Y.; Duncan, R. G.; Hayes, A. N.; Liu, J.; Kasperkovitz, P. V.; Placke, M. E.; Barros, S. A. Exposure to siRNA-GalNAc Conjugates in Systems of the Standard Test Battery for Genotoxicity. *Nucleic Acid Ther.* **2016**, *26* (6), 363–371.

(11) Parmar, R.; Willoughby, J. L.; Liu, J.; Foster, D. J.; Brigham, B.; Theile, C. S.; Charisse, K.; Akinc, A.; Guidry, E.; Pei, Y.; Strapps, W.; Cancilla, M.; Stanton, M. G.; Rajeev, K. G.; Sepp-Lorenzino, L.; Manoharan, M.; Meyers, R.; Maier, M. A.; Jadhav, V. 5'-(E)-Vinylphosphonate: A Stable Phosphate Mimic Can Improve the RNAi Activity of siRNA-GalNAc Conjugates. *ChemBioChem* **2016**, *17* (11), 985–989.

(12) Khvorova, A.; Watts, J. K. The chemical evolution of oligonucleotide therapies of clinical utility. *Nat. Biotechnol.* **2017**, *35* (3), 238–248.

(13) Nair, J. K.; Attarwala, H.; Sehgal, A.; Wang, Q.; Aluri, K.; Zhang, X.; Gao, M.; Liu, J.; Indrakanti, R.; Schofield, S.; Kretschmer, P.; Brown, C. R.; Gupta, S.; Willoughby, J. L. S.; Boshar, J. A.; Jadhav, V.; Charisse, K.; Zimmermann, T.; Fitzgerald, K.; Manoharan, M.; Rajeev, K. G.; Akinc, A.; Hutabarat, R.; Maier, M. A. Impact of enhanced metabolic stability on pharmacokinetics and pharmacodynamics of GalNAc-siRNA conjugates. *Nucleic Acids Res.* **2017**, *45* (19), 10969–10977.

(14) Foster, D. J.; Brown, C. R.; Shaikh, S.; Trapp, C.; Schlegel, M. K.; Qian, K.; Sehgal, A.; Rajeev, K. G.; Jadhav, V.; Manoharan, M.; Kuchimanchi, S.; Maier, M. A.; Milstein, S. Advanced siRNA Designs Further Improve In Vivo Performance of GalNAc-siRNA Conjugates. *Mol. Ther.* **2018**, *26* (3), 708–717.

(15) Janas, M. M.; Harbison, C. E.; Perry, V. K.; Carito, B.; Sutherland, J. E.; Vaishnav, A. K.; Keirstead, N. D.; Warner, G. The Nonclinical Safety Profile of GalNAc-conjugated RNAi Therapeutics in Subacute Studies. *Toxicol. Pathol.* **2018**, *46* (7), 735–745.

(16) Egli, M.; Manoharan, M. Re-Engineering RNA Molecules into Therapeutic Agents. *Acc. Chem. Res.* **2019**, *52* (4), 1036–1047.

(17) Egli, M.; Manoharan, M. Chemistry, structure and function of approved oligonucleotide therapeutics. *Nucleic Acids Res.* **2023**, *51* (6), 2529–2573.

- (18) Janas, M. M.; Schlegel, M. K.; Harbison, C. E.; Yilmaz, V. O.; Jiang, Y.; Parmar, R.; Zlatev, I.; Castoreno, A.; Xu, H.; Shulgamorskaya, S.; Rajeev, K. G.; Manoharan, M.; Keirstead, N. D.; Maier, M. A.; Jadhav, V. Selection of GalNAc-conjugated siRNAs with limited off-target-driven rat hepatotoxicity. *Nat. Commun.* **2018**, *9* (1), No. 723.
- (19) Janas, M. M.; Zlatev, I.; Liu, J.; Jiang, Y.; Barros, S. A.; Sutherland, J. E.; Davis, W. P.; Liu, J.; Brown, C. R.; Liu, X.; Schlegel, M. K.; Blair, L.; Zhang, X.; Das, B.; Tran, C.; Aluri, K.; Li, J.; Agarwal, S.; Indrakanti, R.; Charisse, K.; Nair, J.; Matsuda, S.; Rajeev, K. G.; Zimmermann, T.; Sepp-Lorenzino, L.; Xu, Y.; Akinc, A.; Fitzgerald, K.; Vaishnav, A. K.; Smith, P. F.; Manoharan, M.; Jadhav, V.; Wu, J.-T.; Maier, M. A. Safety evaluation of 2'-deoxy-2'-fluoro nucleotides in GalNAc-siRNA conjugates. *Nucleic Acids Res.* **2019**, *47*, 3306–3320.
- (20) Biscans, A.; Caiazzi, J.; Davis, S.; McHugh, N.; Sousa, J.; Khvorova, A. The chemical structure and phosphorothioate content of hydrophobically modified siRNAs impact extrahepatic distribution and efficacy. *Nucleic Acids Res.* **2020**, *48* (14), 7665–7680.
- (21) (a) Kim, D.-H.; Behlke, M. A.; Rose, S. D.; Chang, M.-S.; Choi, S.; Rossi, J. J. Synthetic dsRNA Dicer substrates enhance RNAi potency and efficacy. *Nat. Biotechnol.* **2005**, *23* (2), 222–226. (b) https://www.accessdata.fda.gov/drugsatfda_docs/label/2023/215842s000lbl.pdf.
- (22) van den Berg, F. T.; Rossi, J. J.; Arbuthnot, P.; Weinberg, M. S. Design of Effective Primary MicroRNA Mimics With Different Basal Stem Conformations. *Mol. Ther. Nucleic Acids* **2016**, *5* (1), No. e278.
- (23) Galka-Marciniak, P.; Olejniczak, M.; Starega-Roslan, J.; Szczesniak, M. W.; Makalowska, I.; Krzyzosiak, W. J. siRNA release from pri-miRNA scaffolds is controlled by the sequence and structure of RNA. *Biochim. Biophys. Acta* **2016**, *1859* (4), 639–649.
- (24) Terasawa, K.; Shimizu, K.; Tsujimoto, G. Synthetic pre-miRNA-based shRNA as potent RNAi triggers. *J. Nucleic Acids* **2011**, *2011*, No. 131579.
- (25) Yu, D.; Pendergraff, H.; Liu, J.; Kordasiewicz, H. B.; Cleveland, D. W.; Swayze, E. E.; Lima, W. F.; Crooke, S. T.; Prakash, T. P.; Corey, D. R. Single-Stranded RNAs Use RNAi to Potently and Allele-Selectively Inhibit Mutant Huntingtin Expression. *Cell* **2012**, *150* (5), 895–908.
- (26) Lima, W. F.; Prakash, T. P.; Murray, H. M.; Kinberger, G. A.; Li, W.; Chappell, A. E.; Li, C. S.; Murray, S. F.; Gaus, H.; Seth, P. P.; Swayze, E. E.; Crooke, S. T. Single-Stranded siRNAs Activate RNAi in Animals. *Cell* **2012**, *150* (5), 883–894.
- (27) Bramsen, J. B.; Laursen, M. B.; Damgaard, C. K.; Lena, S. W.; Babu, B. R.; Wengel, J.; Kjems, J. Improved silencing properties using small internally segmented interfering RNAs. *Nucleic Acids Res.* **2007**, *35* (17), 5886–5897.
- (28) Alterman, J. F.; Godinho, B. M. D. C.; Hassler, M. R.; Ferguson, C. M.; Echeverria, D.; Sapp, E.; Haraszti, R. A.; Coles, A. H.; Conroy, F.; Miller, R.; Roux, L.; Yan, P.; Knox, E. G.; Turanov, A. A.; King, R. M.; Gernoux, G.; Mueller, C.; Gray-Edwards, H. L.; Moser, R. P.; Bishop, N. C.; Jaber, S. M.; Gounis, M. J.; Sena-Estevés, M.; Pai, A. A.; DiFiglia, M.; Aronin, N.; Khvorova, A. A divalent siRNA chemical scaffold for potent and sustained modulation of gene expression throughout the central nervous system. *Nat. Biotechnol.* **2019**, *37* (8), 884–894.
- (29) Hariharan, V. N.; Shin, M.; Chang, C.-W.; O'Reilly, D.; Biscans, A.; Yamada, K.; Guo, Z.; Somasundaran, M.; Tang, Q.; Monopoli, K.; Krishnamurthy, P. M.; Devi, G.; McHugh, N.; Cooper, D. A.; Echeverria, D.; Cruz, J.; Chan, I. L.; Liu, P.; Lim, S.-Y.; McConnell, J.; Singh, S. P.; Hildebrand, S.; Sousa, J.; Davis, S. M.; Kennedy, Z.; Ferguson, C.; Godinho, B. M. D. C.; Thillier, Y.; Caiazzi, J.; Ly, S.; Muhuri, M.; Kelly, K.; Humphries, F.; Cousineau, A.; Parsi, K. M.; Li, Q.; Wang, Y.; Maehr, R.; Gao, G.; Korkin, D.; McDougall, W. M.; Finberg, R. W.; Fitzgerald, K. A.; Wang, J. P.; Watts, J. K.; Khvorova, A. Divalent siRNAs are bioavailable in the lung and efficiently block SARS-CoV-2 infection. *Proc. Natl. Acad. Sci. U.S.A.* **2023**, *120* (11), No. e2219523120.
- (30) Chandela, A.; Ueno, Y. Design, synthesis and evaluation of novel, branched trident small interfering RNA nanostructures for sequence-specific RNAi activity. *RSC Adv.* **2019**, *9* (59), 34166–34171.
- (31) Jahns, H.; Degaonkar, R.; Podbevsek, P.; Gupta, S.; Bisbe, A.; Aluri, K.; Szeto, J.; Kumar, P.; LeBlanc, S.; Racie, T.; et al. Small circular interfering RNAs (sciRNAs) as a potent therapeutic platform for gene-silencing. *Nucleic Acids Res.* **2021**, *49* (18), 10250–10264.
- (32) Chang, C. I.; Yoo, J. W.; Hong, S. W.; Lee, S. E.; Kang, H. S.; Sun, X.; Rogoff, H. A.; Ban, C.; Kim, S.; Li, C. J.; Lee, D. K. Asymmetric shorter-duplex siRNA structures trigger efficient gene silencing with reduced nonspecific effects. *Mol. Ther.* **2009**, *17* (4), 725–732.
- (33) Foster, D. J.; Barros, S.; Duncan, R.; Shaikh, S.; Cantley, W.; Dell, A.; Bulgakova, E.; O'Shea, J.; Taneja, N.; Kuchimanchi, S.; Sherrill, C. B.; Akinc, A.; Hinkle, G.; Seila White, A. C.; Pang, B.; Charisse, K.; Meyers, R.; Manoharan, M.; Elbashir, S. M. Comprehensive evaluation of canonical versus Dicer-substrate siRNA in vitro and in vivo. *RNA* **2012**, *18* (3), 557–568.
- (34) Amarzguioui, M.; Lundberg, P.; Cantin, E.; Hagstrom, J.; Behlke, M. A.; Rossi, J. J. Rational design and in vitro and in vivo delivery of Dicer substrate siRNA. *Nat. Protoc.* **2006**, *1* (2), 508–517.
- (35) Raja, M. A. G.; Katas, H.; Amjad, M. W. Design, mechanism, delivery and therapeutics of canonical and Dicer-substrate siRNA. *Asian J. Pharm. Sci.* **2019**, *14* (5), 497–510.
- (36) Springer, A. D.; Dowdy, S. F. GalNAc-siRNA conjugates: leading the way for delivery of RNAi therapeutics. *Nucleic Acid Ther.* **2018**, *28* (3), 109–118.
- (37) Taxman, D. J.; Moore, C. B.; Guthrie, E. H.; Huang, M. T.-H. Short Hairpin RNA (shRNA): Design, Delivery, and Assessment of Gene Knockdown. In *RNA Therapeutics*; Springer, 2010; pp 139–156.
- (38) Singer, O.; Verma, I. M. Applications of lentiviral vectors for shRNA delivery and transgenesis. *Curr. Gene Ther.* **2008**, *8* (6), 483–488.
- (39) Salomon, W.; Bullock, K.; Lapierre, J.; Pavco, P.; Woolf, T.; Kamens, J. Modified dsRNAs that are not processed by Dicer maintain potency and are incorporated into the RISC. *Nucleic Acids Res.* **2010**, *38* (11), 3771–3779.
- (40) Ge, Q.; Dallas, A.; Ilves, H.; Shorenstein, J.; Behlke, M. A.; Johnston, B. H. Effects of chemical modification on the potency, serum stability, and immunostimulatory properties of short shRNAs. *RNA* **2010**, *16* (1), 118–130.
- (41) Kim, H.; Lee, J. S.; Lee, J. B. Generation of siRNA Nanosheets for Efficient RNA Interference. *Sci. Rep.* **2016**, *6*, No. 25146.
- (42) Abe, N.; Abe, H.; Ito, Y. Dumbbell-shaped nanocircular RNAs for RNA interference. *J. Am. Chem. Soc.* **2007**, *129* (49), 15108–15109.
- (43) Aviñó, A.; Ocampo, S. M.; Perales, J. C.; Eritja, R. Branched RNA: A New Architecture for RNA Interference. *J. Nucleic Acids* **2011**, *2011*, No. 586935.
- (44) Zhang, L.; Liang, D.; Wang, Y.; Li, D.; Zhang, J.; Wu, L.; Feng, M.; Yi, F.; Xu, L.; Lei, L.; Du, Q.; Tang, X. Caged circular siRNAs for photomodulation of gene expression in cells and mice. *Chem. Sci.* **2018**, *9* (1), 44–51.
- (45) Kimura, Y.; Shu, Z.; Ito, M.; Abe, N.; Nakamoto, K.; Tomoike, F.; Shuto, S.; Ito, Y.; Abe, H. Intracellular build-up RNAi with single-strand circular RNAs as siRNA precursors. *Chem. Commun.* **2020**, *56* (3), 466–469.
- (46) Abe, N.; Abe, H.; Ohshiro, T.; Nakashima, Y.; Maeda, M.; Ito, Y. Synthesis and characterization of small circular double-stranded RNAs. *Chem. Commun.* **2011**, *47* (7), 2125–2127.
- (47) Zhang, L.; Liang, D.; Chen, C.; Wang, Y.; Amu, G.; Yang, J.; Yu, L.; Dmochowski, I. J.; Tang, X. Circular siRNAs for Reducing Off-Target Effects and Enhancing Long-Term Gene Silencing in Cells and Mice. *Mol. Ther. Nucleic Acids* **2018**, *10*, 237–244.
- (48) Mirkin, C. A.; Petrosko, S. H. Inspired Beyond Nature: Three Decades of Spherical Nucleic Acids and Colloidal Crystal Engineering with DNA. *ACS Nano* **2023**, *17* (17), 16291–16307.
- (49) Kaviani, S.; Fakhri, H. H.; Asohan, J.; Katolik, A.; Damha, M. J.; Sleiman, H. F. Sequence-Controlled Spherical Nucleic Acids: Gene

Silencing, Encapsulation, and Cellular Uptake. *Nucleic Acid Ther.* **2023**, *33* (4), 265–276.

(50) Nakashima, Y.; Abe, H.; Abe, N.; Aikawa, K.; Ito, Y. Branched RNA nanostructures for RNA interference. *Chem. Commun.* **2011**, *47* (29), 8367–8369.

(51) Nair, B. G.; Zhou, Y.; Hagiwara, K.; Ueki, M.; Isoshima, T.; Abe, H.; Ito, Y. Enhancement of synergistic gene silencing by RNA interference using branched “3-in-1” trimer siRNA. *J. Mater. Chem. B* **2017**, *5* (22), 4044–4051.

(52) Cultrara, C. N.; Shah, S.; Kozuch, S. D.; Patel, M. R.; Sabatino, D. Solid phase synthesis and self-assembly of higher-order siRNAs and their bioconjugates. *Chem. Biol. Drug Des.* **2019**, *93* (6), 999–1010.

(53) Andrews, B. I.; Antia, F. D.; Brueggemeier, S. B.; Diorazio, L. J.; Koenig, S. G.; Kopach, M. E.; Lee, H.; Olbrich, M.; Watson, A. L. Sustainability Challenges and Opportunities in Oligonucleotide Manufacturing. *J. Org. Chem.* **2021**, *86* (1), 49–61.

(54) Siolas, D.; Lerner, C.; Burchard, J.; Ge, W.; Linsley, P. S.; Paddison, P. J.; Hannon, G. J.; Cleary, M. A. Synthetic shRNAs as potent RNAi triggers. *Nat. Biotechnol.* **2005**, *23* (2), 227–231.

(55) Gao, M.; Zhang, Q.; Feng, X. H.; Liu, J. Synthetic modified messenger RNA for therapeutic applications. *Acta Biomater.* **2021**, *131*, 1–15.

(56) Hendel, A.; Bak, R. O.; Clark, J. T.; Kennedy, A. B.; Ryan, D. E.; Roy, S.; Steinfeld, I.; Lunstad, B. D.; Kaiser, R. J.; Wilkens, A. B.; Bacchetta, R.; Tsalenko, A.; Dellinger, D.; Bruhn, L.; Porteus, M. H. Chemically modified guide RNAs enhance CRISPR-Cas genome editing in human primary cells. *Nat. Biotechnol.* **2015**, *33* (9), 985–989.

(57) Haraszti, R. A.; Roux, L.; Coles, A. H.; Turanov, A. A.; Alterman, J. F.; Echeverria, D.; Godinho, B.; Aronin, N.; Khvorova, A. 5'-Vinylphosphonate improves tissue accumulation and efficacy of conjugated siRNAs in vivo. *Nucleic Acids Res.* **2017**, *45* (13), 7581–7592.

(58) Ma, J. B.; Ye, K.; Patel, D. J. Structural basis for overhang-specific small interfering RNA recognition by the PAZ domain. *Nature* **2004**, *429* (6989), 318–322.

(59) Elkayam, E.; Kuhn, C. D.; Tocilj, A.; Haase, A. D.; Greene, E. M.; Hannon, G. J.; Joshua-Tor, L. The structure of human argonaute-2 in complex with miR-20a. *Cell* **2012**, *150* (1), 100–110.

(60) Schirle, N. T.; Sheu-Gruttadauria, J.; MacRae, I. J. Structural basis for microRNA targeting. *Science* **2014**, *346* (6209), 608–613.

(61) Raines, R. T. Ribonuclease A. *Chem. Rev.* **1998**, *98* (3), 1045–1066.

(62) Volkov, A. A.; Kruglova, N. S.; Meschaninova, M. I.; Venyaminova, A. G.; Zenkova, M. A.; Vlassov, V. V.; Chernolovskaya, E. L. Selective protection of nuclease-sensitive sites in siRNA prolongs silencing effect. *Oligonucleotides* **2009**, *19* (2), 191–202.

(63) Vornlocher, H.-P.; Hadwiger, P.; Zimmermann, T. S.; Manoharan, M.; Rajeev, K. G.; Roehl, I.; Akinc, A. Nuclease Resistant Double-Stranded Ribonucleic Acid. U.S. Patent US8334373B2, 2015.

(64) Obexer, R.; Nassir, M.; Moody, E. R.; Baran, P. S.; Lovelock, S. L. Modern approaches to therapeutic oligonucleotide manufacturing. *Science* **2024**, *384* (6692), No. eadl4015.

(65) Flemmich, L.; Bereiter, R.; Micura, R. Chemical Synthesis of Modified RNA. *Angew. Chem., Int. Ed.* **2024**, *63* (22), No. e202403063.

(66) Brown, K. M.; Nair, J. K.; Janas, M. M.; Anglero-Rodriguez, Y. I.; Dang, L. T. H.; Peng, H.; Theile, C. S.; Castellanos-Rizaldos, E.; Brown, C.; Foster, D.; Kurz, J.; Allen, J.; Maganti, R.; Li, J.; Matsuda, S.; Stricos, M.; Chickering, T.; Jung, M.; Wassarman, K.; Rollins, J.; Woods, L.; Kelin, A.; Guenther, D. C.; Mobley, M. W.; Petrulis, J.; McDougall, R.; Racie, T.; Bombardier, J.; Cha, D.; Agarwal, S.; Johnson, L.; Jiang, Y.; Lentini, S.; Gilbert, J.; Nguyen, T.; Chigas, S.; LeBlanc, S.; Poreci, U.; Kasper, A.; Rogers, A. B.; Chong, S.; Davis, W.; Sutherland, J. E.; Castoreno, A.; Milstein, S.; Schlegel, M. K.; Zlatev, I.; Charisse, K.; Keating, M.; Manoharan, M.; Fitzgerald, K.; Wu, J.-T.; Maier, M. A.; Jadhav, V. Expanding RNAi therapeutics to

extrahepatic tissues with lipophilic conjugates. *Nat. Biotechnol.* **2022**, *40* (10), 1500–1508.

(67) Wiegand, D. J.; Rittichier, J.; Meyer, E.; Lee, H.; Conway, N. J.; Ahlstedt, D.; Yurtsever, Z.; Rainone, D.; Kuru, E.; Church, G. M. Template-independent enzymatic synthesis of RNA oligonucleotides. *Nat. Biotechnol.* **2024**, DOI: 10.1038/s41587-024-02244-w.

(68) Corey, D. R.; Damha, M. J.; Manoharan, M. Challenges and Opportunities for Nucleic Acid Therapeutics. *Nucleic Acid Ther.* **2022**, *32* (1), 8–13.

Supplementary Material

Single-Stranded Hairpin Loop RNAs (loopmeRNAs) Potently Induce Gene Silencing through the RNA Interference Pathway

Krishna C. Aluri^{1a}, Dhruvajyoti Datta^{1a}, Scott Waldron^a, Nate Taneja^a, June Qin^a, Daniel P. Donnelly^a, Christopher S. Theile^a, Dale C. Guenther^a, Li Lei,^b Joel M. Harp,^b Pradeep S. Pallan^b, Martin Egli^b, Ivan Zlatev^{a, *}, and Muthiah Manoharan^{a, *}

¹ First authors with equal contribution

^aAlnylam Pharmaceuticals, Inc., Cambridge, MA 02142, USA

^bDepartment of Biochemistry, School of Medicine, Vanderbilt University, Nashville, TN 37232, USA.

* To whom correspondence should be addressed: I.Z. Tel: +1-617-682-4164, Email: izlatev@alnylam.com and M.M. Tel: +1-617-551-8319, Email: mmanoharan@alnylam.com

Table of Contents

Materials and Methods	S2
Major metabolites of siRNA or loopmeRNA	S7
Correlation graph	S8
Crystal structure and modeling studies.....	S12
Metabolites identified in plasma or rat liver homogenate for siRNA or loopmeRNA	S13
References.....	S17

MATERIALS AND METHODS

Synthesis of oligonucleotides

Oligonucleotides were synthesized on a MerMade-12 DNA/RNA synthesizer. Sterling solvents and reagents from Glen Research, 500-Å controlled pore glass (CPG) solid supports from Prime Synthesis, 2'-deoxy nucleoside and 2'-O-TBDMS ribonucleoside 3'-phosphoramidites from Thermo, and 2'-OMe and 2'-F nucleoside 3'-phosphoramidites from Hongene were all used as received. The 2'-OMe-uridine-5'-bis-POM-(*E*) vinyl phosphonate 3'-phosphoramidite was synthesized according to previously published procedures¹, dissolved to 0.15 M in 85% acetonitrile 15% dimethylformamide (DMF), and coupled using standard conditions on the synthesizer. GalNAc CPG support was prepared and used as previously described². Low-water content acetonitrile was purchased from EMD Chemicals. A solution of 0.6 M 5-(*S*-ethylthio)-1*H*-tetrazole in acetonitrile was used as the activator. The phosphoramidite solutions were 0.15 M in acetonitrile with 15% DMF as a co-solvent for 2'-OMe uridine and cytidine. The oxidizing reagent was 0.02 M I₂ in THF/pyridine/water. *N,N*-Dimethyl-*N'*-(3-thioxo-3*H*-1,2,4-dithiazol-5-yl)methanimidamide, 0.09 M in pyridine, was used as the sulfurizing reagent. The detritylation reagent was 3% dichloroacetic acid in dichloromethane. After completion of the solid-phase synthesis, the CPG solid support was washed with 5% (v/v) piperidine in anhydrous acetonitrile three times with 5-min holds after each flow. The support was then washed with anhydrous acetonitrile and dried with argon. The oligonucleotides were then incubated with 28-30% (w/v) NH₄OH, at 35 °C for 20 h. For, VP-containing oligonucleotides, the CPG solid support was incubated with 28-30% (w/v) NH₄OH containing 5% (v/v) of diethylamine at 35 °C for 20 h³. The solvent was collected by filtration, and the support was rinsed with water prior to analysis. After removal from the solid support, 2'-O-TBDMS RNA-containing oligonucleotides were subjected to standard deprotection followed by addition of 37% triethylamine trihydrofluoride and incubation at 45 °C for 2 h. Oligonucleotide solutions of approximately 1 OD₂₆₀ units/mL in 30 – 50 µL were analyzed by LC/ESI-MS on an Agilent 6130 single quadrupole LC/MS system using an XBridge C8 column (2.1 × 50 mm, 2.5 µm) at 60 °C. Buffer A consisted of 200 mM 1,1,1,3,3,3-hexafluoro-2-propanol and 16.3 mM triethylamine in water, and buffer B was 100% methanol. A gradient from 0% to 40% of buffer B over 10 min was followed by washing and recalibration at a flow rate of 0.70 mL/min. The column temperature was 75 °C. All oligonucleotides were purified and desalted and further annealed to form GalNAc-siRNAs as previously described².

In vitro metabolism of loopmeRNA in rat plasma and liver homogenates

In vitro metabolism assays were performed in rat plasma (BioIVT, Cat# CUSTOMBIOFBLD) and liver homogenate (BioIVT, custom order) as described previously⁴. The final reaction mixture consisted of 1 mM MgCl₂, 1 mM MnCl₂, and 2 mM CaCl₂. The loopmeRNAs were incubated at 20 µg/mL with either plasma or liver homogenate. The reaction mixture was incubated by gently shaking at 37 °C for 24 h. The reaction was stopped by adding 450 µL of Clarity OTX lysis loading buffer (Phenomenex, Cat# AL0-8579) containing internal standard (oligonucleotide U₂₁ at 1 µg/mL final concentration) and frozen at -80 °C until analysis.

Clarity OTX 96-well solid-phase extraction plates were used to enrich the oligonucleotide from the reaction mixture as described by Liu et. al.⁵ The samples were loaded onto solid-phase extraction columns preconditioned with methanol. Columns were washed with 50 mM ammonium acetate with 2 mM sodium azide in HPLC-grade water and then with 50 mM ammonium acetate in water/acetonitrile (1:1, v/v), pH 5.5. Oligonucleotides were eluted with 10 mM EDTA, 100 mM ammonium bicarbonate in acetonitrile/tetrahydrofuran/water (4:1:5, v/v/v), pH 8.8. The eluant was dried under nitrogen and resuspended in 120 µL of LC-MS grade water for LC-MS analysis.

An aliquot of 30 µL of sample was injected on to Waters X-Bridge BEH C8 XP Column (Cat# 176002554, 130 Å, 2.5 µm, 2.1 mm x 30 mm, 80 °C) and separated using a gradient of 16 mM triethylamine. After a gradient of 1% mobile phase B to 35% B over 4.3 min, the column was equilibrated with 1% mobile phase B for 1 min. Data were acquired using full scan mode on a Thermo Scientific Q Exactive mass spectrophotometer. Data were acquired with a scan range of 500-3000 m/z at a resolution setting of 70,000. The spray voltage was 2.8 kV. The auxiliary gas temperature and the capillary temperature were set to 300 °C. Data were processed using ProMass HR Deconvolution software (Novatia) to identify metabolites as described by Liu et. al.⁵

Analysis of gene silencing in mice

All procedures involving mice were conducted by certified laboratory personnel using protocols consistent with local, state, and federal regulations. Experimental protocols were approved by the Institutional Animal Care and Use Committee (IACUC), the Association for Assessment and Accreditation of Laboratory Animal Care International (accreditation number: 001345), and the Office of Laboratory Animal Welfare (accreditation number: A4517-01). When deciding on sample numbers for animal studies, we determined the final number required to ensure confidence in the resulting data while utilizing the least number of animals as required by IACUC guidelines. Female C57BL/6 mice approximately 8 weeks of age were obtained from Charles River Laboratories and randomly assigned to each group. Mice were acclimated in-house for 48 h before the study started.

Animals were dosed subcutaneously at 10 $\mu\text{L/g}$ with loopmeRNA, siRNA, or with vehicle (PBS, pH 7.4). The doses of loopmeRNA and siRNA used in this study were 0.2, 0.4, and 1 mg/kg. The test compounds were diluted into PBS, pH 7.4. All solutions were stored at 4 $^{\circ}\text{C}$ until the time of injection. Blood was collected utilizing the retro-orbital eye bleed procedure as per the IACUC-approved protocol. The sample was collected into Becton Dickinson serum separator tubes (Fisher Scientific, Cat# BD365967).

For analysis of TTR, serum samples were kept at room temperature for 1 h and then spun in a microcentrifuge at 21,000 $\times g$ at room temperature for 10 min. Serum was transferred into 1.5-mL microcentrifuge tubes for storage at -80 $^{\circ}\text{C}$ until the time of assay. Serum samples were diluted at 1:4,000 and assayed using a commercially available kit from ALPCO specific for the detection of mouse prealbumin (Cat# 41-PALMS-E01), and the manufacturer's instructions were followed. Protein concentrations ($\mu\text{g/mL}$) were determined by comparison to a purified TTR standard.

Correlation analysis

Correlation analysis was performed using GraphPad Prism 8.4.3. Pearson's correlation was performed to correlate either intensity of parent loopmeRNA or antisense 22/23-mer formed with TTR knockdown and two-tailed P value was calculated. P values of less than 0.05 were considered statistically significant.

Crystal structure of the human Ago2 PAZ domain in complex with an RNA nonamer

Protein construct. The amino acid sequences of the human Ago1 and Ago2 PAZ domains (A225-S369 and A227-S371, respectively) are 89% identical (Figure S3). Some of the non-conserved amino acids map to the binding site for the 3'-terminal nucleotide of the siRNA guide strand (FigureS3). Based on the Ago1 PAZ protein used for determining the crystal structure of its complex with RNA (A225-S369),⁶ we produced Ago2 PAZ comprised of amino acids A227-S371⁷. However, co-crystallization experiments with the same RNA 9mer 5'-CGU GAC UCU-3' used for determining the structure of the Ago1 PAZ:RNA complex, only gave crystals of the apo-form of Ago2 PAZ that diffracted to 3.5 Å. We noticed that residues 350-369 that were part of the Ago1 PAZ protein were not visible in the structure of that complex (PDB ID 1SI3; <http://www.rcsb.org>) (Figure S4). Subsequently, we omitted the corresponding residues in the expression system for the human Ago2 PAZ domain.

Expression. The codon optimized gene for PAZ residues 227-352 was produced by GenScript and cloned into the pHD116 vector with an N-terminal cleavable His₆ tag. *E. coli* BL21 (DE3) Gold or BL21(DE3) PlysS cells were co-transformed with the vectors containing the PAZ and pGro12 ES/EL genes. Cell cultures were grown in an incubator/shaker at 37 °C and at 175–225 r.p.m. Chaperones were induced by the addition of 1-2 mg/ml arabinose, and target protein expression was induced by the addition of IPTG to a final concentration of 1 mM. Cells were harvested by centrifuging for 25 min at 3000 r.p.m. and 4 °C and then discarding the supernatant. The cell pellet was resuspended in 80-100 mL of 100 mM Tris buffer pH 8.0 or TES buffer pH 8.0 with the addition of lysozyme to 1 mg/ml. Centrifugation and removal of supernatant were repeated, and cells stored at -80 °C.

Purification and His tag cleavage. Following sonication and addition of 0.1% polyethyleneimine and centrifugation, the supernatant was collected, and the PAZ domain purified by Nickel-affinity chromatography. The His tag was cleaved using HRV 3C (PreScission) protease. The sample was then kept at 4 °C overnight, followed by Q and S fast-flow sepharose column chromatography, and passage through small GST and Ni columns. If found to be of insufficient purity at this stage, the PAZ domain was

further purified by gel filtration chromatography. For crystallization experiments, the human Ago2 PAZ domain was concentrated to 10 mg/mL (Figure S5).

Crystallization. A solution of 10 mg/mL PAZ mixed with RNA 9-mer at 1:1.2 ratio was kept on ice for 2-3 hours before setting up droplets with the Index Screen (Hampton Research). Crystals were obtained by sitting drop vapor diffusion from Index solutions 39, (i.e., 100 mM HEPES pH 7.0 and 30% v/v Jeffamine) and 57 in three days. Hexagonal rods obtained from solution IN39 are depicted in Figure S5.

X-ray diffraction data collection and processing. Diffraction data for were collected on the 21-ID-D beam line of the Life Sciences Collaborative Access Team (LS-CAT) at the Advanced Photon Source (APS), located at Argonne National Laboratory (Argonne, IL), using an Eiger 9M detector. The wavelength was tuned to 0.9184 Å, and crystals were kept at 100 K during data collection. Data were integrated, scaled and merged with xia2 using the DIALS software package.⁸ Selected crystal data and processing statistics are listed in Table S1.

Phasing and refinement. Data were phased by the molecular replacement method with the program Molrep⁹ in the CCP4 suite of crystallographic software¹⁰ using the human Ago1 PAZ domain as the search model (PDB ID 1SI3). Following initial positional and isotropic temperature factor refinement cycles with the program Refmac5,¹¹ the orientation of the RNA molecule was clear in Fourier ($2F_o - F_c$) sum and ($F_o - F_c$) difference electron density maps, and the RNA molecule was built into the density with the program Coot.¹² At this stage, refinement was continued and the R-work/R-free values dropped to around 32%. Further refinement in Refmac5¹¹ and addition of water molecules resulted in reasonable figures of merit. Final refinement parameters are listed in Table S1, and the quality of the final electron density is depicted in Figure 6. While this work was underway the crystal structure of an Ago2 PAZ complex with RNA was published¹³.

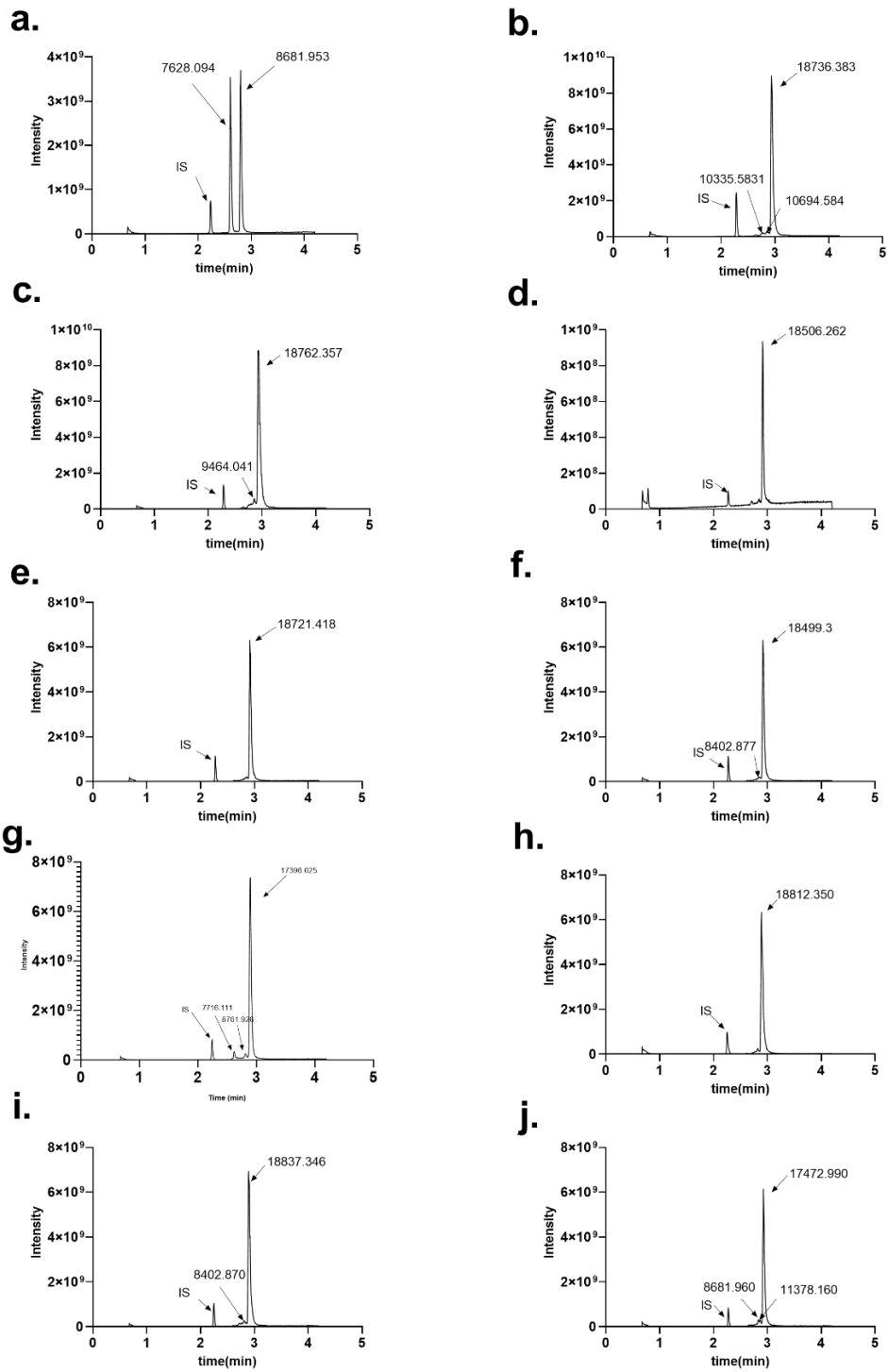


Figure S1: Total ion chromatograms showing major metabolites of siRNA or loopmeRNA formed at 24 hours in rat plasma. **a.** ON-1, **b.** ON-2, **c.** ON-3, **d.** ON-5, **e.** ON-6, **f.** ON-7, **g.** ON-8, **h.** ON-9, **i.** ON-10, and **j.** ON- 11

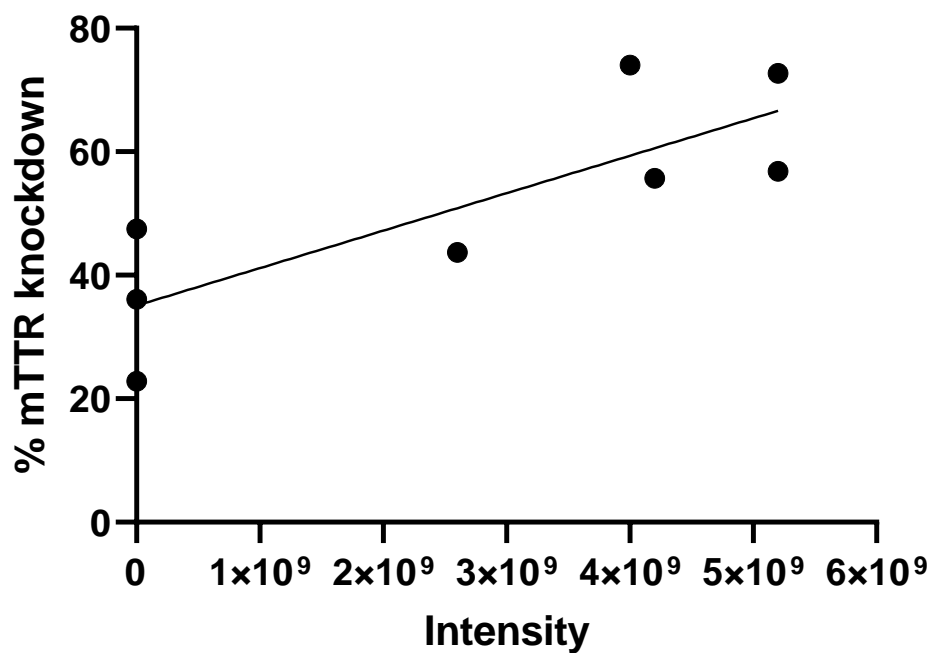


Figure S2. Percent TTR reduction in vivo inversely correlates with the amount of antisense strand metabolite. Plot of TTR remaining at day 7 in mice treated with 0.2 mg/kg dose of loopmeRNA vs. signal intensity due to antisense strand metabolite detected after incubation in rat liver homogenate for 24 h.

a. **Range 1: 23 to 859** [Graphics](#) ▼ Next Match

Score	Expect	Method	Alignment statistics for match #1	Identities	Positives
1498 bits(3878)	0.0	Compositional matrix adjust.		703/838(84%)	777/838(92%)
Query 21	FQAPRRPGIGTVGKPIKLLANYFEVDIPKIDVYHYEVDIKPKDCPRRVNREVVEYMQHF				80
Sbjct 23	F+ P RP GT G+ IKL AN+FE+DIPKID+YHYE+DIKP+KCPRRVNRE+VE+MVQHF				82
Query 81	KPQIFGDRKPVYDGKKNYITVTALPIGNERVDFEVTIPGEGKDRIFKVSIKWLAIVSWRM				140
Sbjct 83	K QIFGDRKPV+DG+KN+YT LPIG ++V+ EVT+PGEKDRIFKVSIKW++ VS +				142
Query 141	LHEALVSGQIP-VPLESVQALDVAMRHLASMRYPVGRSFFSPPEGYHPLGGGREVWFG				199
Sbjct 143	LH+AL SG++P VP E++QALDV MRHL SMRYTPVGRSFF+ EG +PLGGGREVWFG				201
Query 200	FHQSVRPAMWKMLNIDVSATAFYKAQPVIEFMCVLDIRNIDEQPKPLTDSQVRVFTKE				259
Sbjct 202	FHQSVRP++WKMLNIDVSATAFYKAQPVIEF+CEVLD ++I+EQ KPLTDSQRV+FTKE				261
Query 260	IKGLKVEVTHCGQMKRKYRVCNVTRRPASHQTFPLQLESGQTVECTVAQYFKQKYNLQLK				319
Sbjct 262	IKGLKVE+THCGQMKRKYRVCNVTRRPASHQTFPLQ ESGQTVECTVAQYFK ++ L L+				321
Query 320	YPHLPCLQVQEQKHLYLPLEVCNIVAGQRCIKKLTDNQTSTMIKATARSAPDRQEEISR				379
Sbjct 322	YPHLPCLQVQEQKHLYLPLEVCNIVAGQRCIKKLTDNQTSTMI+ATARSAPDRQEEIS+				381

b.

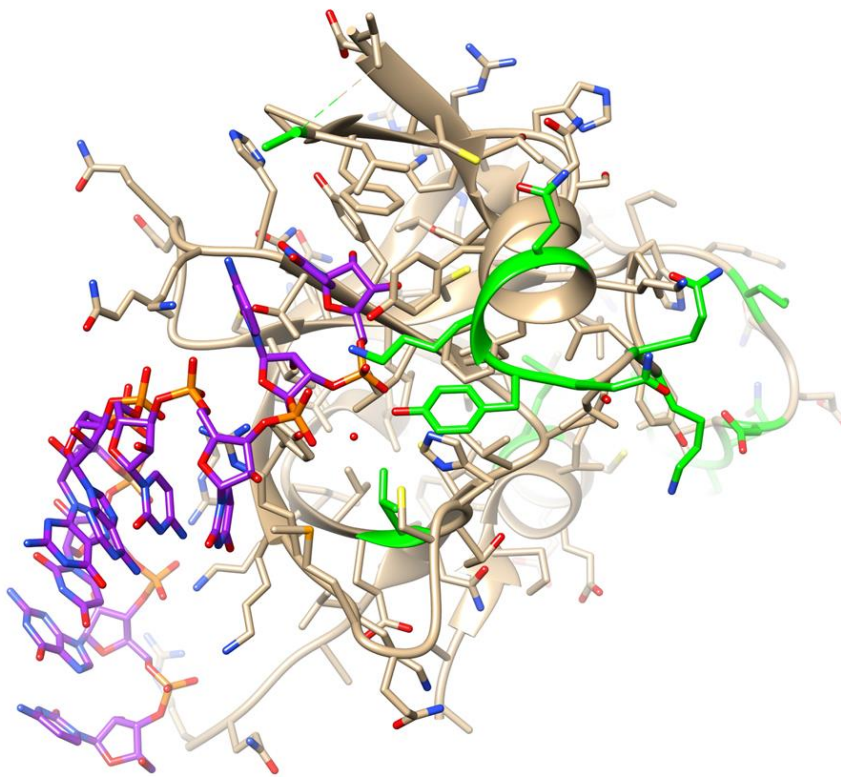


Figure S3. a. Sequence alignment for the human Ago1 (top) and Ago2 (bottom) PAZ domains (regions highlighted in red). b. Crystal structure of the Ago1 PAZ domain in complex with an RNA 9mer⁶ (PDB 1S13). The protein backbone is shown as a ribbon with side chain carbon, oxygen, nitrogen, and sulfur atoms colored in tan, red, blue, and yellow, respectively. Oligoribonucleotide carbon, oxygen, nitrogen, and phosphorus atoms are colored in purple, red, blue, and orange, respectively. Amino acids highlighted in green in the structure of Ago1 PAZ differ from those in Ago2 PAZ.

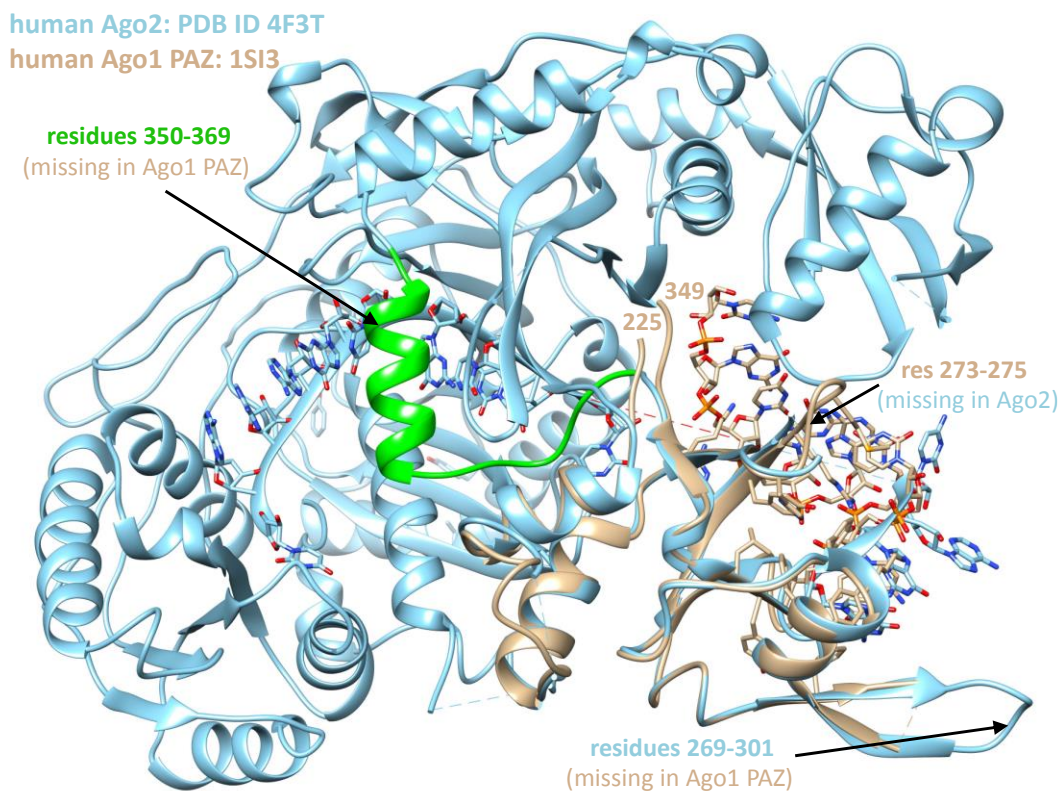


Figure S4. Overlay of the crystal structure of human Ago1 PAZ in complex with RNA⁶ (PDB ID 1S13; beige) and the PAZ domain from the crystal structure of human Ago2 in complex with miR-20a¹⁴ (PDB ID 4F3T; light blue). Arrows point to protein (loop) regions missing in the respective structures. Although contained in the protein expressed for co-crystallization with RNA, residues highlighted in green in human Ago1 PAZ (350-369) were not observed in the electron density.

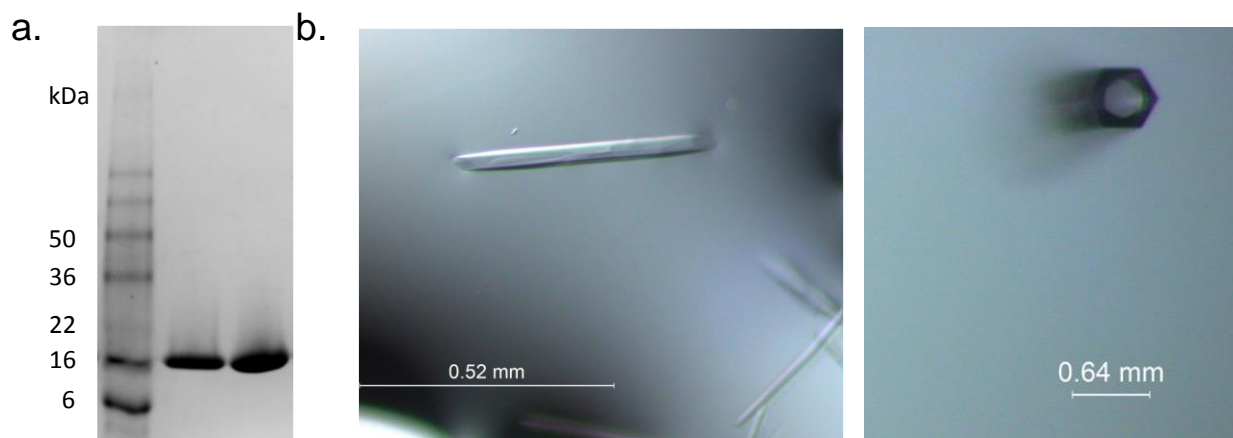


Figure S5. a. Purity of the human Ago2 PAZ domain (4-12% SDS-PAGE). b. Crystals of the complex between Ago2 PAZ and the RNA 9mer 5'-CGU GAC UCU-3' from Index screen solution 39.

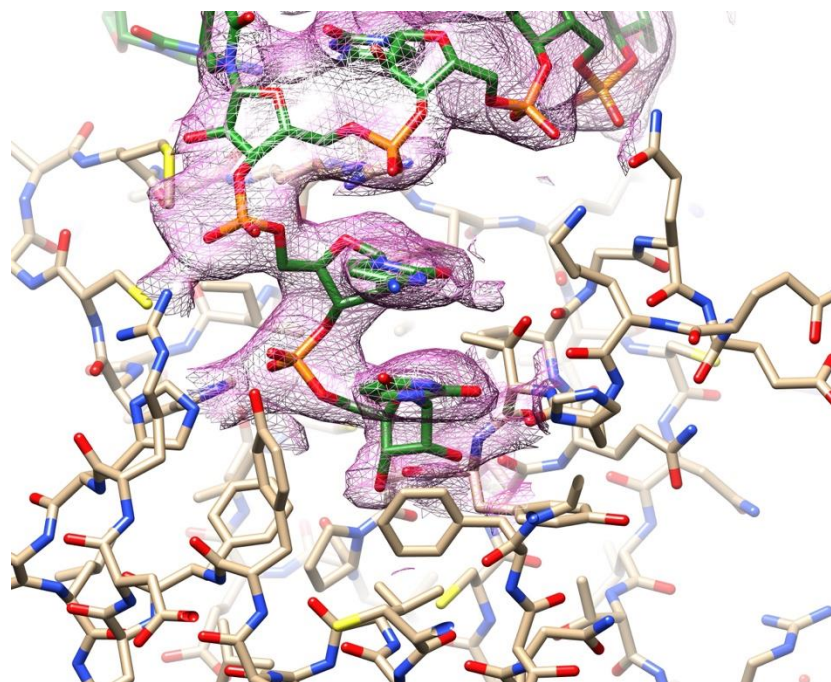


Figure S6. Quality of the final $2F_o-F_c$ sum electron density around RNA atoms (1σ threshold).

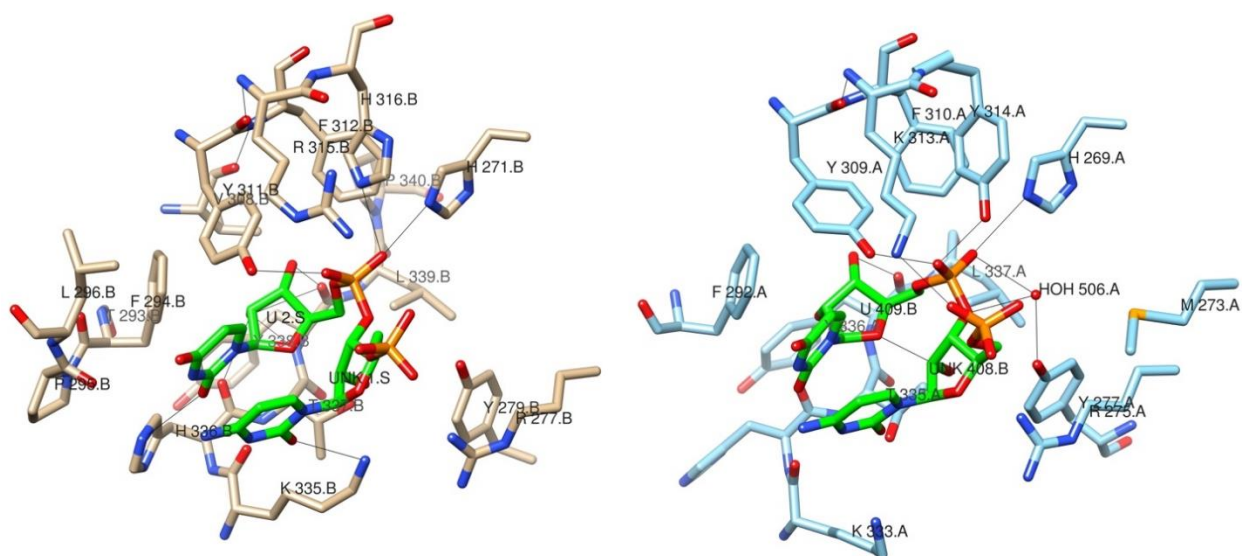


Figure S7. Comparison between the binding modes of 3'-terminal CU overhangs by the human Ago2 PAZ (left, this work) and human Ago1 PAZ domains (right; PDB ID 1SI3).⁶ Protein side chains are labeled, and H-bonds and salt bridges are indicated by thin solid lines.

Table S1. Crystal structure of the Ago2 PAZ:RNA complex. Selected crystal data, data collection and refinement parameters.

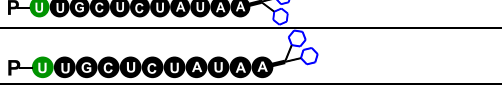
Crystal data	
Resolution [Å]	46.23 - 2.41
Space group	<i>P6₅</i>
PAZ/RNA molecules per a.u.	2 / 2
Unit cell <i>a</i> , <i>b</i> , <i>c</i> [Å]; α , β , γ [deg.]	91.94, 91.94, 69.58; 90.00, 90.00, 120.00
Data collection	
No. of unique reflections	13,092 (1,301) ^a
Resolution [Å]	2.41 (2.50 - 2.41)
Completeness [%] (last shell)	100.0 (100.0)
R-merge	0.091 (1.026)
R-pim (last shell)	0.021 (0.226)
I/ σ I	31.5 (1.2)
Refinement	
R-work / R-free	0.215 / 0.284
Number of protein atoms	1,979
Number of RNA atoms	354
No. of water molecules	16
Average B factor [Å ²]	
Protein atoms	63.5
RNA atoms	99.9
Water molecules	46.9
R.m.s. deviations:	
Bond lengths [Å]	0.005
Bond angles [°]	1.5
Data deposition	
PDB ID code	8THQ

^aNumbers in parentheses refer to the outermost shell.

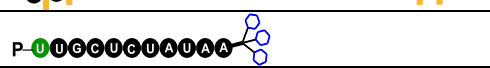
Table S2: Metabolites identified in plasma for siRNA or loopmeRNA

	Mass (Da)	Sequence	Residue Identifier*
ON-1	8681.953		Parent-sense
	7628.094		Parent-antisense
ON-2	18736.383		Parent
	13335.583		1-31
	10694.584		1-32
ON-3	18762.357		Parent
	9464.041		29-52
ON-5	18506.261		Parent
ON-6	18721.418		Parent
ON-7	18499.3		Parent
	8402.3.877		32-52
ON-8	17396.025		Parent
	8761.926		27-48
	7716.111		9-44
ON-9	188812.35		Parent
ON-10	18762.357		Parent
	9464.041		29-52
ON-11	17472.99		Parent
	11378.160		2-35
	8681.960		28-49

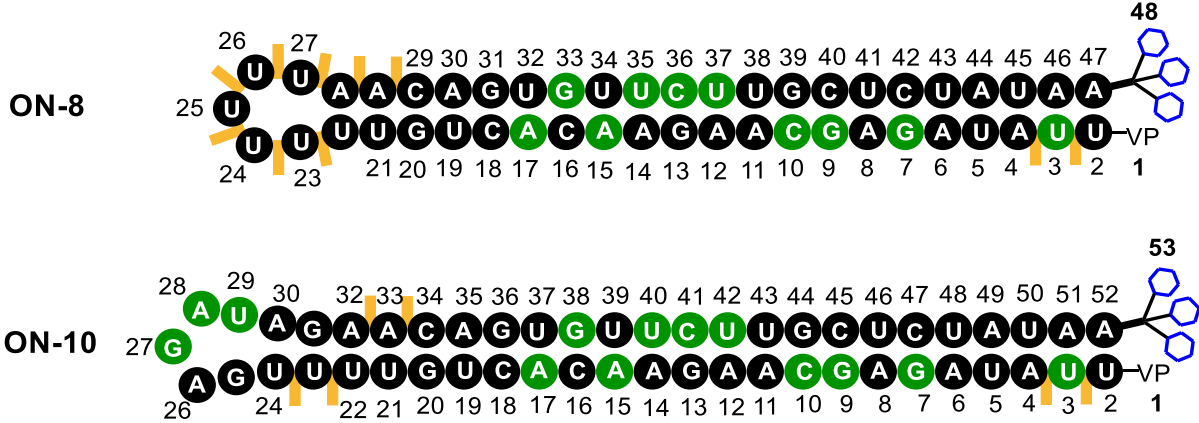
Table S3: Metabolites identified in rat liver homogenate for siRNA or loopmeRNA at 24 hours

	Mass (Da)	Sequence	Residue Identifier*
ON-1	8681.953		Parent-sense
	8478.873		
	5420.473	P-UUGCUCUAUAA 	11-22
	7628.094		Parent-antisense
ON-2	18736.383		Parent
	13333.92		1-40
	13026.881		1-39
	5420.396	P-UUGCUCUAUAA 	41-52
	5217.396	P-UUGCUCUAUAA 	41-52
ON-3	18762.357		Parent
	8761.9585	P-AACAGUGUUCUUGCUCUAUAA 	31-52
	9120.979	P-GAACAGUGUUCUUGCUCUAUAA 	30-52
	9384.08		13-40
	9464.0896	P-AAGAACAGUGUUCUUGCUCUAUAA 	29-52
	7628.095		1-23
	5420.472	P-UUGCUCUAUAA 	41-52
	5217.396	P-UUGCUCUAUAA 	41-52
ON-5	9065.963	P-TAACAGUGUUCUUGCUCUAUAA 	30-52
	8862.887	P-TAACAGUGUUCUUGCUCUAUAA 	30-52
	7628.093		1-23
	5217.395	P-UUGCUCUAUAA 	41-52
	3663.50		5-15
ON-6	18721.418		Parent
	13319.958		10-49
	5420.474	P-UUGCUCUAUAA 	41-52
	5217.396	P-UUGCUCUAUAA 	41-52

	7628.096	UUUUGUCACAAAGAACGAGAUUU	1-23
ON-7	18499.3	T T T T A A C A G U G U C U U G C U C U A U A A T T U U U U G U C A C A A G A A C G A G A U A U U	Parent
	9065.965	T T T T A A C A G U G U C U U G C U C U T T U U U U -P	20-47
	8761.919	P - A A C A G U G U C U U G C U C U A U A A	31-52
	7628.095	U U U U G U C A C A A G A A C G A G A U A U U	1-23
	3663.50	C A A G A A C G A G A	5-15
ON-8	17396.025	U U A A C A G U G U C U U G C U C U A U A A U U U U G U C A C A A G A A C G A G A U A U U	Parent
	17193.938	U U A A C A G U G U C U U G C U C U A U A A U U U U G U C A C A A G A A C G A G A U A U U	Parent-1GalNAc
	11993.57	U U A A C A G U G U C U U G C U C U A U U U U U G U C A C A A G A A -P	10-45
	5420.473	P - U U G C U C U A U A A	37-48
	5217.393	P - U U G C U C U A U A A	37-48
	5317.828	A G A A G A A C G A G A U A U U	1-16
ON-9	188812.35	U U A G A A C A G U G U C U U G C U C U A U A A A G U U U U G U C A C A A G A A C G A G A U A U U -VP	Parent
	18609.277	U U A G A A C A G U G U C U U G C U C U A U A A A G U U U U G U C A C A A G A A C G A G A U A U U -VP	Parent-GalNAc
	13409.894	U U A G A A C A G U G U C A G U U U U G U C A C A A G A A C G A G A U A U U -VP	1-41
	13102.863	U U A G A A C A G U G U U A G U U U U G U C A C A A G A A C G A G A U A U U -VP	1-40
	5420.472	P - U U G C U C U A U A A	42-53
	5217.395	P - U U G C U C U A U A A	42-53
ON-10	18837.346	A U A C A A C A G U G U C U U G C U C U A U A A G A G U U U U G U C A C A A G A A C G A G A U A U U -VP	Parent
	9384.061	A G A A C A G U G U C U U G C U C U A U A A	30-53
	9120.981	P - G A A C A G U G U C U U G C U C U A U A A	31-53
	8761.918	P - A A C A G U G U C U U G C U C U A U A A	32-53
	9464.05	P - A G A A C A G U G U C U U G C U C U A U A A	30-53
	9772.068	P - U A G A A C A G U G U C U U G C U C U A U A A	29-53
	7704.066	U U U U G U C A C A A G A A C G A G A U A U U -VP	1-24
	5217.396	P - U U G C U C U A U A A	42-53
	5014.319	P - U U G C U C U A U A A	42-53

ON-11	17472.99		Parent
	12070.539		1-37
	11454.486		1-35
	5420.472		37-48

*Residue identifier illustrated for ON-8 and ON-10



References:

1. Parmar, R. G.; Brown, C. R.; Matsuda, S.; Willoughby, J. L. S.; Theile, C. S.; Charissé, K.; Foster, D. J.; Zlatev, I.; Jadhav, V.; Maier, M. A.; Egli, M.; Manoharan, M.; Rajeev, K. G., Facile Synthesis, Geometry, and 2'-Substituent-Dependent in Vivo Activity of 5'-(E)- and 5'-(Z)-Vinylphosphonate-Modified siRNA Conjugates. *J. Med. Chem.* **2018**, *61* (3), 734-744.
2. Nair, J. K.; Willoughby, J. L.; Chan, A.; Charisse, K.; Alam, M. R.; Wang, Q.; Hoekstra, M.; Kandasamy, P.; Kel'in, A. V.; Milstein, S.; Taneja, N.; O'Shea, J.; Shaikh, S.; Zhang, L.; van der Sluis, R. J.; Jung, M. E.; Akinc, A.; Hutabarat, R.; Kuchimanchi, S.; Fitzgerald, K.; Zimmermann, T.; van Berkel, T. J.; Maier, M. A.; Rajeev, K. G.; Manoharan, M., Multivalent N-acetylgalactosamine-conjugated siRNA localizes in hepatocytes and elicits robust RNAi-mediated gene silencing. *J. Am. Chem. Soc.* **2014**, *136* (49), 16958-61.
3. O'Shea, J.; Theile, C. S.; Das, R.; Babu, I. R.; Charisse, K.; Manoharan, M.; Maier, M. A.; Zlatev, I., An efficient deprotection method for 5'-[O,O-bis(pivaloyloxymethyl)]-(E)-vinylphosphonate containing oligonucleotides. *Tetrahedron* **2018**, *74* (42), 6182-6186.
4. Jahns, H.; Degaonkar, R.; Podbevsek, P.; Gupta, S.; Bisbe, A.; Aluri, K.; Szeto, J.; Kumar, P.; LeBlanc, S.; Racie, T. et.al., Small circular interfering RNAs (sciRNAs) as a potent therapeutic platform for gene-silencing. *Nucleic Acids Res.* **2021**, *49* (18), 10250-10264.
5. Liu, J.; Li, J.; Tran, C.; Aluri, K.; Zhang, X.; Clausen, V.; Zlatev, I.; Guan, L.; Chong, S.; Charisse, K.; Wu, J. T.; Najarian, D.; Xu, Y., Oligonucleotide quantification and metabolite profiling by high-resolution and accurate mass spectrometry. *Bioanalysis* **2019**, *11* (21), 1967-1980.
6. Ma, J. B.; Ye, K.; Patel, D. J., Structural basis for overhang-specific small interfering RNA recognition by the PAZ domain. *Nature* **2004**, *429* (6989), 318-322.
7. Seo, M.; Lei, L.; Egli, M., Label-Free Electrophoretic Mobility Shift Assay (EMSA) for Measuring Dissociation Constants of Protein-RNA Complexes. *Curr. Protoc. Nucleic Acid Chem.* **2019**, *76* (1), e70.
8. Beilsten-Edmands, J.; Winter, G.; Gildea, R.; Parkhurst, J.; Waterman, D.; Evans, G., Scaling diffraction data in the DIALS software package: algorithms and new approaches for multi-crystal scaling. *Acta Crystallogr. D Struct. Biol.* **2020**, *76* (Pt 4), 385-399.
9. Vagin, A.; Teplyakov, A., MOLREP: an Automated Program for Molecular Replacement. *J. Appl. Crystallogr.* **1997**, *30* (6), 1022-1025.
10. Winn, M. D.; Ballard, C. C.; Cowtan, K. D.; Dodson, E. J.; Emsley, P.; Evans, P. R.; Keegan, R. M.; Krissinel, E. B.; Leslie, A. G.; McCoy, A.; McNicholas, S. J.; Murshudov, G. N.; Pannu, N. S.; Potterton, E. A.; Powell, H. R.; Read, R. J.; Vagin, A.; Wilson, K. S., Overview of the CCP4 suite and current developments. *Acta Crystallogr. D Biol. Crystallogr.* **2011**, *67* (Pt 4), 235-42.
11. Murshudov, G. N.; Skubák, P.; Lebedev, A. A.; Pannu, N. S.; Steiner, R. A.; Nicholls, R. A.; Winn, M. D.; Long, F.; Vagin, A. A., REFMAC5 for the refinement of macromolecular crystal structures. *Acta Crystallogr. D Biol. Crystallogr.* **2011**, *67* (Pt 4), 355-67.
12. Emsley, P.; Cowtan, K., Coot: model-building tools for molecular graphics. *Acta Crystallogr. D Biol. Crystallogr.* **2004**, *60* (Pt 12 Pt 1), 2126-32.
13. Greenidge, P. A.; Blommers, M. J. J.; Priestle, J. P.; Hunziker, J., How to Computationally Stack the Deck for Hit-to-Lead Generation: In Silico Molecular Interaction Energy Profiling for de Novo siRNA Guide Strand Surrogate Selection. *J. Chem. Info. Model.* **2019**, *59* (5), 1897-1908.

14. Elkayam, E.; Kuhn, C.-D.; Tocilj, A.; Haase, Astrid D.; Greene, Emily M.; Hannon, Gregory J.; Joshua-Tor, L., The Structure of Human Argonaute-2 in Complex with miR-20a. *Cell* **2012**, *150* (1), 100-110.